Overstory and understory leaves warm faster than air in evergreen needleleaf forests

Keenan Ganz[1*], Christopher J. Still[2], Bharat Rastogi[3], L. Monika Moskal[1]

[1]School of Environmental and Forest Sciences, University of Washington, Seattle WA 98195

[2]Department of Forest Ecosystems and Society, Oregon State University, Corvallis OR 97333

[3]Department of Geography, University of Colorado, Boulder CO 80309

* Corresponding author; ganzk@uw.edu

Abstract

The limited homeothermy hypothesis states that leaves maintain their temperature within an optimal range for photosynthesis by increasing transpiration during warm conditions. Under limited homeothermy, plants may offset thermal stress caused by climate change. If this hypothesis is true, we should observe: 1) leaf temperature increasing slower than air temperature and 2) leaves cooler than air during warm conditions. We tested these predictions with an energy balance model for evergreen needleleaf forest sites in the National Ecological Observatory Network. A key feature of our model was its vertical stratification of the canopy, which allowed us to analyze vertical gradients in canopy temperature. This feature is especially important given that prior work has focused on the tops of forest canopies. Our results do not support limited homeothermy at any canopy position. In all canopy strata, leaf temperature increased faster than air and periods with leaves cooler than air were rare. In such cases, cooling was due to emitted radiation, not transpiration. But, when water was abundant, transpiration could produce mildly homeothermic behavior. We attribute these results to the needle-like shape of leaves in our study sites. This leaf shape increases boundary layer conductance and causes heat gain from surrounding air to overpower heat loss from transpiration when leaves are cooler than air. Our results indicate that needleleaf forests cannot avert thermal stress in a warming world. Thermal limits on photosynthesis and non-linear increases in respiration with temperature may weaken the role of evergreen forests as a global carbon sink.

Keywords: leaf temperature, canopy temperature, homeothermy, energy balance, photosynthesis, respiration

1 Introduction

From molecules to ecosystems, temperature is key to understanding plant physiology. At the molecular scale, higher temperatures increase membrane fluidity, chemical reaction rate, enzyme activity and solute diffusivity (Jones, 2013). At the leaf scale, increases in temperature imply faster gas exchange due to enhanced thermodiffusion (Griffani et al., 2024). At the whole-plant scale, seasonal canopy temperature forcing drives multiple phenological transitions and can cause tissue damage if low- or high-temperature thresholds are reached (Körner and Hiltbrunner, 2018). Environmental conditions and biological properties shape leaf temperature dynamics. Air temperature, vapor pressure deficit, shortwave radiation, and other microclimate parameters regulate the energy balance of a leaf (Jones, 2013), while plant and ecosystem traits, like canopy structure, exert control over leaf temperature through the radiation budget, sensible heat exchange, and moisture availability (Javadian et al., 2022; Kibler et al., 2023; Vinod et al., 2023). Environmental conditions and plant traits determine the energy balance of a plant, its productivity, and its ability to tolerate stress.

The importance of temperature in so many aspects of plant physiological function raises a broad question about climate change: will the thermal regime of terrestrial plants amplify or dampen heat and drought stress from climate change? This question is important because drought and heat stress reduces carbon uptake by inducing stomatal closure (Choat et al., 2018). If these effects are globally widespread, many forests may consume more water to maintain current carbon uptake or transition from being carbon sinks to carbon sources (Williams et al., 2016).

One proposed plant response to mitigating thermal stress is the limited homeothermy hypothesis. This hypothesis states that plants, in analogy with ectothermic animals, can maintain their photosynthetic tissues within an optimal temperature range by increasing transpiration

during periods of thermal stress, sufficient soil moisture, low atmospheric humidity, and high net radiation (Mahan and Upchurch, 1988). Early work supported this hypothesis in irrigated agricultural settings, for example with cotton (Upchurch and Mahan, 1988) and corn (Gardner et al., 1981). Meta-analyses across plant species also lent support to limited homeothermy. Linacre (1964) found that the threshold for leaves becoming cooler than air was around 33 °C for well-watered plants exposed to the sun. More recently, Michaletz et al. (2016) applied similar methods to a compilation of literature data and found a leaf-on-air temperature slope of 0.74, with some plants as much as 20 K cooler than air. However, it is not clear whether these plants were measured under well-watered conditions. Regardless, these studies suggested that plants consistently exhibit limited homeothermy if sufficient moisture is available to support transpiration. Limited homeothermy may not directly apply to natural ecosystems because the hypothesis was originally developed in irrigated agricultural settings, for example with cotton (Upchurch and Mahan, 1988) and corn (Gardner et al., 1981) which have very high intrinsic stomatal conductance compared to non-agricultural plants.

Further research at larger spatial scales and in field conditions has generally contradicted the limited homeothermy hypothesis outside of agricultural settings and certain hyper-arid plants with adaptations for shedding solar radiation and heat load (Lin et al., 2017). Temperate needleleaf and broadleaf trees have both been observed several degrees warmer than air under field conditions (Leuzinger and Körner, 2007; Aubrecht et al., 2016; Kim et al., 2018). Scherrer et al. (2011) considered the effect of species and drought status in a deciduous forest and found that canopy temperatures rose to 3 K above air following drought. Although initial work found that leaves could be cooler than air under certain conditions, later work has found that these

conditions are rare in natural ecosystems. Thus, leaves are rarely cooler than air in uncontrolled conditions.

Thermal remote sensing in forests has also shown how canopy structure determines leaf temperature by altering wind patterns and attenuating radiation. Leuzinger and Körner (2007) first observed leaf temperature varying more than 10 K within a single tree canopy. Miller et al. (2021) and Garen et al. (2023) examined the vertical dimension: in a wet tropical forest, upper-canopy leaves exceeded air temperature, while lower-canopy leaves tracked closely with air temperature. Javadian et al. (2022) examined the horizontal dimension: in a semi-arid conifer forest during the afternoon, upper-canopy leaves in high-density stands were cooler than air while upper-canopy leaves in low-density stands were warmer than air. These differences arose from self-shading in the canopy that reduced the radiation load for a particular leaf. In general, the three-dimensional structure of a forest canopy creates gradients in microclimate and leaf traits that determine how much and in what form energy reaches leaves (Vinod et al., 2023).

Still et al. (2022) and Guo et al. (2023a) revisited the limited homeothermy hypothesis with thermal remote sensing at two scales. Still et al. (2022) utilized data from thermal cameras installed on eddy covariance towers across forest ecosystems in North America and found no evidence of limited homeothermy. Instead, tree canopies warmed as much as 40% faster than air. Using a simple leaf energy balance model, Still et al. (2022) also noted that for forest canopies to cool below air temperature, latent heat fluxes from transpiration would have to exceed absorbed radiation. These conditions imply a negative sensible heat flux, which was not observed at any of the sites they studied during the daytime. Guo et al. (2023a) combined satellite land-surface temperature with climate reanalysis data to investigate limited homeothermy in a wide range of ecosystems. They found that land-surface temperature did not exhibit limited homeothermy in

80% of pixels and that environmental drivers of land-surface temperature were only apparent after removing the air temperature signal (i.e., using $\Delta T = T_{LST} - T_A$ instead of T_{LST}).

Besides remote sensing, another tool to study the temperature of plants is leaf energy balance modeling. Leaf energy balance models calculate leaf temperature by balancing incoming and outgoing energy flux for a leaf, usually under steady state conditions. Assuming steady state and ignoring stored heat, the energy balance of a leaf is

$$R_n - H - \lambda E = 0 \text{ [W m}^{-2}\text{]}, \quad (1)$$

where R_n is absorbed shortwave and longwave radiation, H is sensible heat flux, and λE is latent heat flux (a full list of symbols and values for constants is in Table S1, and the units for each equation in the manuscript are annotated in square brackets). If canopy microclimate and leaf physiology are known, Eq. (1) is solved numerically.

Energy balance models are useful for several applications, including determining the drivers of observed leaf temperature (Muller et al., 2021), sensitivity analysis (Vinod et al., 2023), and evaluating a hypothesized relationship among plant traits (Michaletz et al., 2016; Okajima et al., 2012). The main downside of energy balance models is that they require a number of parameters, thus, many types of data are necessary to parameterize modeled fluxes, and even with extensive instrumentation, simplifying assumptions of leaf geometry, spectral properties, and steady-state conditions may be necessary.

Once leaf temperature data are collected, multiple approaches to characterizing the leaf thermal regime have been proposed. The limited homeothermy hypothesis is drawn from the animal physiology literature, and within that framework temperature regimes have been classified based on the slope of the leaf-air temperature relationship (β) or the leaf-air temperature difference (ΔT). Leaves are megathermic if they warm faster than air ($\beta > 1$, $\Delta T >$

123 0), poikilothermic if they warm at the same rate as air ($\beta \approx 1$, $\Delta T \approx 0$), and homeothermic if
124 they warm slower than air ($\beta < 1$, $\Delta T < 0$) (Blonder and Michaletz, 2018; Cavaleri, 2020; Still et
125 al., 2023a). Leaves warming faster than air would amplify thermal stress from climate change,
126 while leaves warming slower than air would dampen thermal stress. A decoupling of leaf and air
127 temperature ($\beta \neq 1$ or $\Delta T \neq 0$) may also disrupt photosynthesis and alter the role of evergreen
128 forests as a terrestrial carbon sink by increasing respiration or damaging photosynthetic tissue.
129 Categorizing leaf thermal regime by the leaf-air temperature slope enables comparison
130 among sites, but obscures underlying temperature drivers. Another framework to describe leaf
131 temperature regimes involves decomposing leaf temperature into forcings from net radiation
132 warming and transpiration cooling. This 3-T method (Michaletz et al., 2016; Zhou et al., 2023)
133 compares three related temperatures: leaf temperature (T_L), air temperature (T_A), and the
134 temperature of a non-transpiring leaf analog (T_{NT}). The value of T_{NT} may be determined either
135 by measuring the temperature of a leaf covered in petroleum jelly (Idso et al., 1981; Zhou et al.,
136 2023) or with a leaf energy balance model where stomatal conductance is set to zero. With these
137 three temperatures, temperature forcings from net radiation and transpiration can be derived as
138 follows. Net radiation forcing is the difference between the non-transpiring leaf temperature and
139 air temperature ($T_{NT} - T_A$), while transpiration forcing is the difference between actual leaf
140 temperature and non-transpiring leaf temperature ($T_L - T_{NT}$). Changes in ΔT and β could be due
141 to reduced transpiration, increased net radiation, or both. By decomposing ΔT, the 3-T method
142 provides insight into which aspect of a leaf's thermal regime determines a change in leaf
143 temperature.
144 Previous investigations involving the above frameworks have, however, focused on
145 measurements at the canopy top. This is because tower-mounted cameras and spaceborne sensors

mainly view the tops of canopies, which are most exposed and therefore most vulnerable to thermal stress. Uncertainty remains over the thermal regime of within-canopy leaves. Our study addresses this knowledge gap to improve our understanding of how thermal stress will influence the entire canopy of a forest.

Here, we sought to evaluate the limited homeothermy hypothesis across canopy profiles in a range of North American evergreen needleleaf forests. The vertical dimension is important since constraints on leaf function can vary significantly within the canopy (Vinod et al., 2023). However, since vertical radiation and microclimate gradients both heat and cool lower canopy leaves relative to the upper canopy, their overall effect is unclear. On one hand, lower-canopy leaves would be cooled by less intense and longer wavelength radiation. On the other hand, lower-canopy leaves would be warmed by increased relative humidity, slower wind speed, and longwave radiation from soil. Most research to date has focused on upper-canopy leaves only, although there is some evidence of poikilothermic leaves in tropical sub-canopies (Garen et al., 2023; Miller et al., 2021). Given that the majority of canopy foliage is shaded, the behavior of lower-canopy leaves is critical to our understanding of thermal regimes in forests.

We focused on evergreen needleleaf forests because of methodological constraints, limited data, and because these forests face increased aridity (Williams et al., 2019), thermal stress from heatwaves (Still et al., 2023b), and drought-induced tree mortality (Anderegg et al., 2013; Choat et al., 2018) due to climate change. All of these disturbances threaten to transform evergreen forests from carbon sinks into carbon sources (Liu et al., 2024). Of course, broadleaf forests experience these disturbances too, but we excluded broadleaf forests because our analysis rests on assumptions of forest structure that are more valid in needleleaf than broadleaf forests (see section 2.4).

To address whether limited homeothermy occurs and its potential impact on canopy function, we studied evergreen needleleaf forests from the US-based National Ecological Observatory Network (NEON; https://www.neonscience.org/). These sites (Table 1 and Figure 1) occupy a broad climate space and provide a wide range of canopy structure. We posed the following questions:

1. Is there evidence of limited homeothermy in evergreen needleleaf forests?
2. How much of temperature forcing is governed by the physical environment of a leaf versus leaf transpiration?

To answer these questions, we developed a multi-layer leaf energy balance model in seven evergreen needleleaf forests monitored by NEON. This model was used to estimate leaf temperature using energy balance theory and accounting for vertical gradients in forest structure. We then compared our model output against expectations of limited homeothermy ($\beta < 1, \Delta T < 0$) and compared leaf temperature forcings from radiation and transpiration using the 3-T method at each layer.

2 Methods

2.1 Site selection

We used sites from NEON, where diverse data on canopy structure, physiology, and microclimate is routinely collected. Importantly, vertical profiles of canopy microclimate enabled us to calibrate our multi-layer model. Here, we used sites where evergreen needleleaf trees are dominant overstory vegetation type and where data quality was sufficient for model calibration. These sites are listed in Table 1 and their sensor arrangements are shown in Figure 1.

Table 1: Characteristics of NEON sites used in this study. Coordinates are for the eddy covariance flux tower at each site. Note that canopy heights differ from NEON sources because our heights describe the canopy in the immediate vicinity of the flux tower at each site. Leaf area indices shown here come from literature or MODIS data as follows, a: MODIS; b: Gough et al. (2019); c: Still et al. (2021).

Site name	Site code	Latitude (°)	Longitude (°)	Forest characteristics	Canopy height (m)	Leaf area index
Abby Road, WA	ABBY	45.76	-122.33	Second-growth Douglas fir with western hemlock	14	3.80[a]
Delta Junction, AK	DEJU	63.88	-145.75	Stunted black spruce and white spruce	10	1.70[a]
Jones Environmental Research Center, GA	JERC	31.19	-84.47	Longleaf pine with deciduous hardwoods	23	4.20[a]
Ordway-Swisher Biological Station, FL	OSBS	29.69	-81.99	Longleaf and loblolly pine with deciduous hardwoods	21	2.50[b]
Rocky Mountain National Park, CO	RMNP	40.28	-105.55	Ponderosa pine with juniper and Douglas fir	17	2.00[a]
Talladega National Forest, AL	TALL	32.95	-87.39	Longleaf and loblolly pine with deciduous hardwoods	24	4.80[b]

Wind River Experimental Forest, WA	WREF	45.82	-121.95	Old-growth Douglas fir with western hemlock	58	9.20[c]

NEON sites are outfitted with infrared radiometers that record canopy biological temperature (T_{bio}) at multiple vertical positions (Figure 1). These narrow-field-of-view radiometers (SI-111; Apogee Instruments, Logan, UT) record data at 1 Hz, and NEON manages aggregation of these high-frequency data to match the half-hourly observation interval of other data products (https://data.neonscience.org/data-products/DP1.00005.001). Observations of T_{bio} are not necessarily equal to leaf temperature because T_{bio} is a composite temperature influenced by both leaves and non-leaf background like soil and bark. Although biological temperature is comparable to leaf temperature, a non-leaf background is typically warmer than leaves and can bias such biological temperature measurements (Aubrecht et al., 2016; Pau et al., 2018; Still et al., 2019a). We utilized T_{bio} for model validation despite its potential bias because alternative within-canopy observations of leaf temperature were not available. Whether a particular radiometer accurately records leaf temperature depends on its orientation and the structure of the canopy. If we assume that non-leaf background is warmer than leaves, then we would expect our modeled leaf temperatures to be cooler but well correlated with T_{bio}. We also excluded radiometers within 2 m of the ground since these most likely measured soil temperature instead of canopy T_{bio}. Due to these limitations in T_{bio}, validation with T_{bio} served to help us understand potential bias in our model but not to evaluate its accuracy.

In addition to T_{bio}, microclimate data are recorded at multiple vertical positions in each site (Figure 1). These data enabled us to account for vertical gradients in microclimate and transpiration in our model. Thus, our study sites are not only well instrumented for energy

balance modeling but also let us explore how the energy balance and leaf temperature dynamics of evergreen needleleaf forests change across canopy layers.

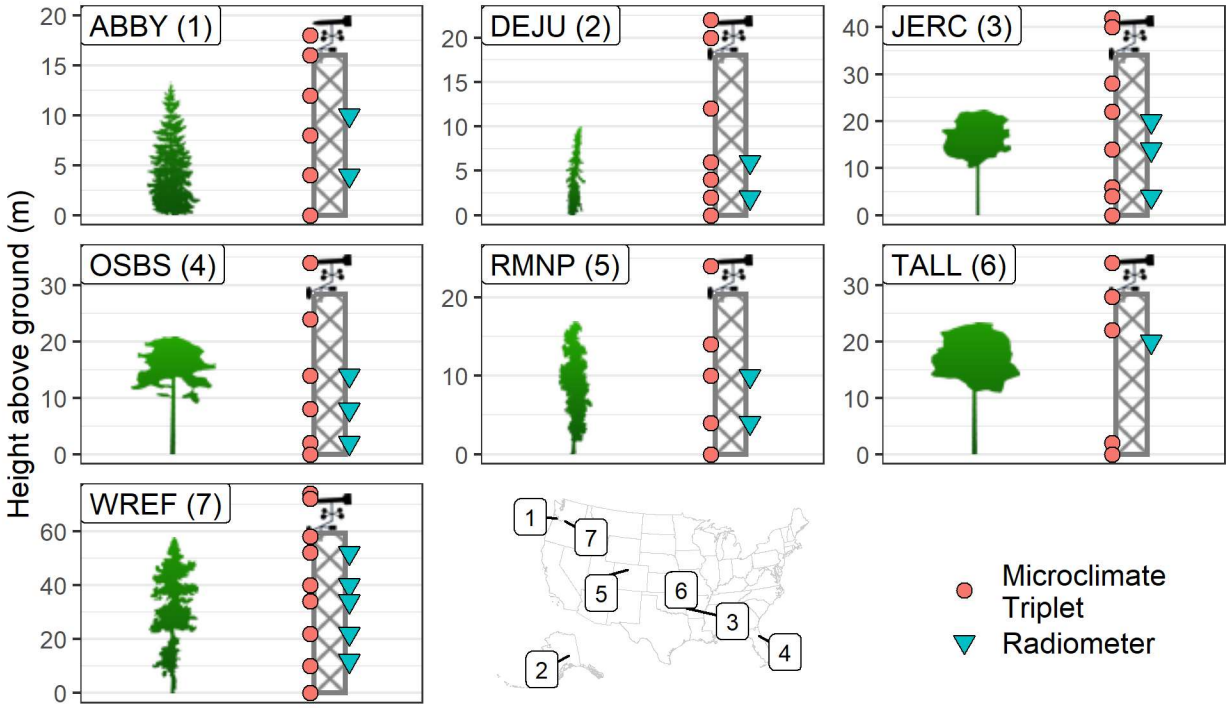

Figure 1: Vertical position of microclimate triplets (red circles) and canopy radiometers (blue triangles). Numbers in parentheses correspond to locations on the site map in lower center panel. "Microclimate triplet" refers to air temperature, humidity, and wind speed sensors collocated within 1 m of each other. Tree and tower graphics are to scale but note varying y-axis limits among panels.

2.2 Model overview

We extended the leaf-level energy balance model in Eq. (1) to study leaf temperature at different vertical positions in a forest canopy. The steady-state assumption is valid here because needle leaves reach thermal equilibrium much faster than the half-hourly timestep in our source data (Jones, 2013; Michaletz et al., 2016). We represented each study site as a sequence of layers with constant leaf area index (LAI) but varying vertical thickness. In each layer, we assumed steady-state conditions and solved Eq. (1) independently of all other layers with microclimate

data and a calibration procedure outlined in Figure 2. First, we determined canopy LAI and the number of layers to model in each site with MODIS LAI imagery. Then, we used aerial light detection and ranging (lidar) to determine the appropriate thickness and height of each layer (Figure S4). Since layer positions were not necessarily collocated with microclimate sensors, we interpolated microclimate data vertically to match the height of each layer. Next, we attributed canopy-scale fluxes measured by an eddy covariance tower to each model layer according to the layer microclimate and calibrated constants. Therefore, our modeling of leaf-level photosynthesis is a top-down approach that does not consider processes necessary in a bottom-up approach, like leaf-level metabolism, canopy nitrogen distribution, and soil moisture. These simplifications made our model easier to run but did not compromise its ability to model energy balance.

We draw a distinction between the terms “canopy” and “leaf,” whose definitions vary elsewhere in the literature. Here, “canopy” refers to all overstory foliage in each site, while “leaf” or “layer” refers to some vertical slice of the canopy. Our approach models the temperature of a leaf experiencing the conditions of a particular position in a forest canopy. Since we do not consider horizontal heterogeneity, “leaves” represent an average across all foliage in each canopy layer.

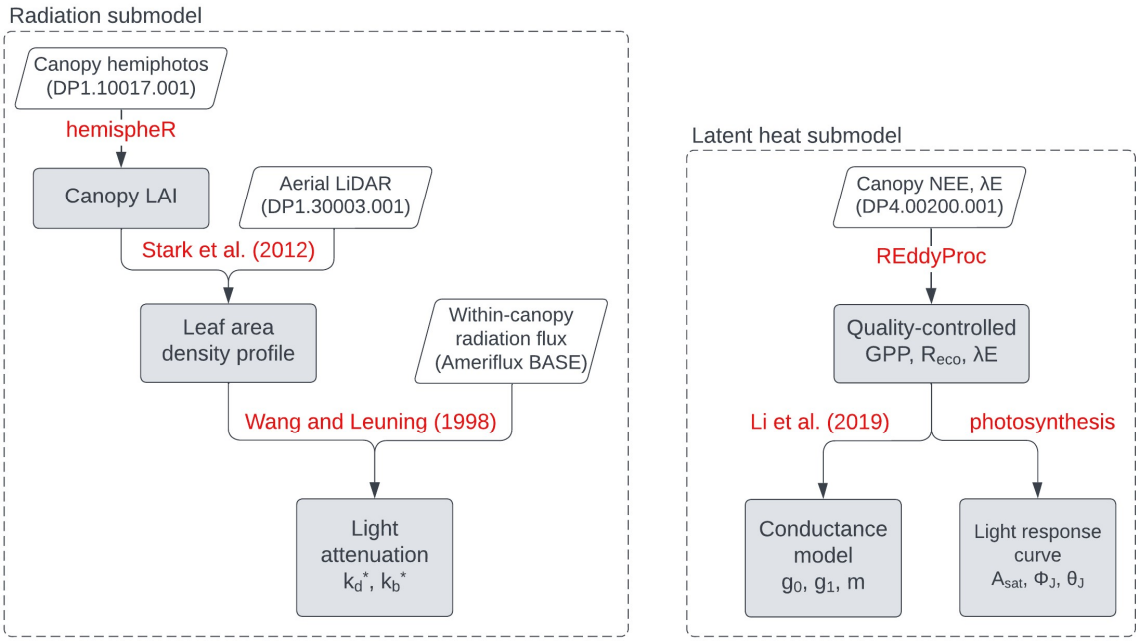

247

248 Figure 2: Overview of model calibration steps. Leaf-level sensible heat flux in Eq. (1) was
249 derived from microclimate data and is omitted for brevity. Skewed rectangles represent raw data
250 sources from NEON or Ameriflux, while shaded rectangles represent derived data products. Red
251 annotations cite either method descriptions in the literature or R packages used to implement the
252 associated process.

253 Calibrated model constants are shown in leaf nodes in Figure 2. These constants describe
254 how our model represented light attenuation (k_d^*, k_b^*), stomatal conductance (g_0, g_1, m), and
255 photosynthesis (A_{sat}, Φ_J, θ_J) in each site. Once calibrated, the energy balance model required the
256 following inputs: air temperature, relative humidity, wind speed, canopy gross primary
257 production (GPP), and top-of-canopy radiation flux. Meteorological inputs are recorded at
258 multiple positions in the canopy. Where necessary, we interpolated these inputs to match the
259 vertical position of layers in our model. Other inputs, like top-of-canopy radiation and GPP, are
260 not recorded throughout the canopy. In these cases, we estimated their distribution through the
261 canopy (see sections 2.4 and 2.5). Our results are therefore limited to half-hour observation
262 periods where all the above inputs were available. We also filtered input data to daylight hours

from May – September in each site, which roughly corresponds to the growing season at these sites. During the growing season, forest canopies in these sites are most active physiologically and most likely to experience thermal stress. Therefore, this period is when we would expect to observe limited homeothermy in the lower canopy.

Our model depends upon a simplified representation of canopy photosynthesis (section 2.5) and radiation absorption (section 2.4). These simplifications are possible because of two assumptions. In particular, we assumed a spherical leaf angle distribution to simplify radiation calculations and comparable light response between sun and shade leaves to simplify photosynthesis calculations. To test the validity of these assumptions, we conducted a sensitivity analysis with respect to leaf conductance and canopy transpiration. We also compared our results with other model predictions in the literature. These analyses provide confidence that our conclusions about leaf thermal regimes are robust to these assumptions.

2.3 Site leaf area index

Our analysis began with determining LAI for each site. At three sites, we used LAI values from literature sources (Table 1). We initially tried using hemispheric photographs from NEON to determine LAI, but we found poor agreement with literature values (data not shown). Instead, we extracted LAI from the MODIS LAI product MCD15A2H. We sampled all images from May to September and from 2018 to 2022 and then took the median value for each site as its LAI for our analysis. In the three sites where literature data were available, these values for LAI took precedence over values from MODIS imagery.

We acknowledge that assuming LAI is constant prevents us from capturing the effect of disturbance or growth on leaf temperature. We accepted this uncertainty because we primarily used LAI to determine the number of layers to include in our model. Therefore, our LAI

calculations need only be accurate to the nearest whole number. NEON did not report any disturbances in our study sites that would have caused a significant drop in LAI during the study period (https://data.neonscience.org/data-products/DP1.10111.001). However, ABBY was clearcut in 2017 and experienced rapid growth during the study period. In ABBY, LAI likely increased over the period we modeled, and the value used here should be interpreted as an average over this period.

Site LAI determined how many canopy layers we included in each site. We rounded each LAI value up to the nearest integer and took this result as the number of canopy layers except for DEJU. In DEJU, canopy LAI was low enough that we would only model one canopy layer. Since we developed our study to evaluate how leaf temperature varied across vertical strata, we decided to model two layers in DEJU. Model layers were not evenly distributed throughout the canopy. Instead, we used aerial lidar within 50 m of the eddy covariance tower at each site to generate a leaf area density profile after Stark et al. (2012) and placed layers at heights that corresponded to integer values of cumulative LAI (Figure S4). Note that in this procedure we excluded lidar returns within 1 m of the ground. In this way, each model layer acted as a layer of foliage with LAI equal to one.

We then modeled the energy budget at each canopy layer with Eq. (1) to determine leaf temperature. In text, we also refer to cumulative LAI, which is the number of layers above a particular layer. Cumulative LAI is equal to zero at the canopy top, then increases by one for each layer lower in the canopy. When visualizing our results, we divided the canopy into lower, middle, and upper sections. We defined the lower canopy as the lowermost layer in the model, the upper canopy as the uppermost layer in the model, and the middle canopy as all other model layers.

2.4 Net absorbed radiation

We calculated net absorbed radiation in each canopy layer as

$$R_n = SW_{abs} + \epsilon_f LW_{dn} - \epsilon_f \sigma T_L^4 \text{ [W m}^{-2}\text{]}, \quad (2)$$

where SW_{abs} is absorbed shortwave radiation, LW_{dn} is downwelling longwave radiation, ϵ_f is leaf emissivity, σ is the Stefan-Boltzmann constant, and T_L is leaf temperature. Previous studies, such as Still et al. (2022), used an isothermal form of R_n. Doing so simplifies the procedure for calculating T_L but implies that $T_L = T_A$ in the radiation term, which is inappropriate in our evaluation of whether leaf temperature deviates from air temperature.

We calculated SW_{abs} for each layer according to Eq. (B2) and Eq. (B3) in Wang and Leuning (1998). These equations use a modified Beer-Lambert relationship that accounts for scattering, soil reflectance, and solar angle. We assumed a spherical leaf angle distribution and constant values for leaf emissivity, leaf scattering coefficient, soil emissivity, and canopy reflection coefficient as listed in Table S1.

After making the above assumptions, two empirical coefficients in Wang and Leuning (1998) required calibration: k_d^* and k_b^*. These coefficients described how diffuse and beam shortwave radiation fluxes, respectively, attenuate in a real canopy according to the Beer-Lambert law. Although top-of-canopy radiation sensors in our study sites distinguish between diffuse and beam radiation, within-canopy radiation sensors do not. Therefore, we adopted a modified Beer-Lambert law to describe the combined attenuation of diffuse and beam shortwave radiation within the canopy:

$$SW_z / SW_{top} = \exp(-[k_b^* \cdot (1 - f) + k_d^* \cdot f] \cdot z) \text{ [}-\text{]}, \quad (3)$$

where SW_z is the total shortwave radiation flux at the layer with cumulative LAI z, SW_{top} is the total shortwave radiation flux at the top of the canopy, and f is the proportion of diffuse shortwave radiation at the top of the canopy.

We solved for k_d^* and k_b^* using within-canopy radiation sensors in three steps. First, we determined the cumulative LAI at each radiation sensor using the same leaf area density profiles we created when determining model layers. Second, we binned half-hourly radiation observations at each sensor in 10% increments of f and calculated the geometric mean of SW_z/SW_{top}. Finally, we linearized Eq. (3) by taking the natural logarithm of both sides and solved for k_d^* and k_b^* using ordinary least squares regression. We found that diffuse light attenuated less than beam light in all sites (Figure S1).

We calculated LW_{dn} according to Eq. (B8) in Wang and Leuning (1998). This equation models changes in the effective emissivity of the leaf surroundings through the canopy. At the canopy top, LW_{dn} is equal to the downwelling flux recorded by top-of-canopy sensors. Deeper in the canopy, LW_{dn} is equal to the blackbody radiance of the surrounding air. Our approach modeled canopy layers independently, so longwave radiation fluxes from neighboring layers were not considered. No empirical constants required calibration for the longwave radiation term. We note that Eq. (B8) in Wang and Leuning (1998) calls for a sky emissivity, which we calculated as the ratio of top-of-canopy downwelling longwave radiation (LW_{top}) to the blackbody radiance of air at the temperature measured at the top of the canopy,

$$\epsilon_{sky} = LW_{top}/\sigma T_A^4\ [-]. \quad (4)$$

2.5 Latent heat

We modeled latent heat flux following Jarvis and McNoughton (1986) as a mixture of two endpoints,

$$\lambda E = \Omega \lambda E_{eq} + (1 - \Omega)\lambda E_{imp}\ [\mathrm{W\ m^{-2}}], \quad (5)$$

where the total flux (λE) is the sum of equilibrium latent heat (λE_{eq}) and stomatally imposed latent heat (λE_{imp}) weighted by the leaf-air decoupling coefficient (Ω) that ranges from 0 – 1. When leaves are fully decoupled from air ($\Omega = 1$), transpiration is limited by available radiation. When leaves are fully coupled with air ($\Omega = 0$), transpiration is limited by stomatal conductance. The value of Ω is determined by canopy microclimate and stomatal conductance (Monteith and Unsworth, 2013; Still et al., 2022). We note that Ω is a leaf-scale decoupling coefficient, so canopy-scale parameters like surface roughness are not used in its calculation. For brevity, we refer the reader to Monteith and Unsworth (2013), Still et al. (2022), and Supplementary Information for details on calculating λE_{eq}, λE_{imp}, and Ω.

The stomatally imposed endpoint λE_{imp} is calculated by first estimating stomatal conductance (g_s). Since g_s is not measured at NEON sites across canopy layers, we used a generalized stomatal conductance model (Li et al., 2019) to estimate a canopy-scale conductance (G_c; Eq. (6) as a function of GPP, top-of-canopy vapor pressure deficit, top-of-canopy CO_2 mole fraction, and three empirical constants (g_0, g_1, and m):

$$G_c = g_0 + \frac{g_1}{VPD^m}\frac{\mathrm{GPP}}{[\mathrm{CO_2}]}\ [\mathrm{mol\ m^{-2}\ s^{-1}}]. \quad (6)$$

This model formulation accounts for the dependence of water consumption on VPD such that the parameter g_1 is inversely related to intrinsic water-use efficiency (Medlyn et al., 2017) and represents soil evaporation with the parameter g_0. The curvature parameter m allows the dependence on VPD to shift across ecosystems. Our calculation of VPD differed when applying Eq. (6) at canopy scale versus layer scale. At canopy scale, we calculated VPD as the "ecosystem scale VPD" given in Eq. (2) in Li et al. (2019). At layer scale, we calculated VPD from leaf

temperature and ambient relative humidity to capture the gradient in vapor pressure from within the leaf to outside the leaf boundary layer.

We fit Eq. (6), with net ecosystem exchange data from NEON. Although these data do not go through the same processing pipeline as the Ameriflux FLUXNET product, we had to use fluxes from NEON because the FLUXNET product was not available for all of our study sites at the time of analysis. We began by downloading net ecosystem exchange data from NEON and discarding all observations with nonzero quality-control flags. Then, we used the R package REddyProc (Wutzler et al., 2018) to partition net ecosystem exchange into GPP and ecosystem respiration and then fit g_1 with robust nonlinear regression (Maechler et al., 2024). After partitioning flux, we did not include any gap-filled data in further analysis and discarded periods where GPP < 0. When fitting g_1 we discarded observations within 24 hours of a rainfall event to ensure the latent heat flux signal was not affected by intercepted precipitation. Also, due to data limitations, we fit g_1 to all data available for each site instead of repeating the fit annually.

Once g_1 was fit at the canopy scale, we had to estimate gross photosynthesis in each layer to estimate g_s with Eq. (6). We initially assumed that gross photosynthesis in each layer was proportional to the amount of shortwave radiation reaching the layer. This naïve approach would overestimate photosynthesis in the upper canopy if top-of-canopy shortwave radiation exceeds the light saturation point. Therefore, we also accounted for light saturation by fitting light response curves to the relationship between canopy GPP and top-of-canopy downwelling shortwave radiation (Figure S3; Marshall and Biscoe, 1980; Stinziano et al., 2021). In the fitting process, we discarded observations where top-of-canopy shortwave radiation was less than 50 W m^{-2} since fluxes were unreliable in low light.

These light response curves were used to estimate layer photosynthesis based on the light incident on each layer. We estimated the amount of shortwave radiation in each layer with our radiation sub-model (see section 2.4) and then calculated the photosynthesis rate of each layer with the fitted light response curve. Since the light response curves describe canopy-scale GPP, we could not use these curves to describe a single canopy layer directly. Instead, we normalized the photosynthesis rate of each layer so that they summed to the value estimated at the canopy top. Then, we attributed canopy GPP to each model layer based on the amount of light reaching each layer. Finally, we used layer GPP and interpolated microclimate conditions in Eq. (6) to estimate stomatal conductance in each model layer. An example of this calculation is provided in Supplementary Information. Note that since g_0 is assumed to describe soil evaporation, we set this value to zero when calculating leaf-level stomatal conductance even though our canopy-scale analysis had $g_0 > 0$ in all sites.

Our treatment of GPP had the advantage of forcing model canopy GPP to match eddy covariance GPP, but the disadvantage of assuming that sun and shade leaves had the same light response curve. This assumption may not necessarily be true in high-LAI forests such as WREF (Jiang et al., 2019; Kerhoulas et al., 2020; Winner et al., 2004).

2.6 Leaf-level sensible heat

Leaf-level sensible heat flux was calculated from canopy microclimate data in each layer. We adopted a parameterization of this flux for needle leaves as in prior work (Michaletz et al., 2016; Still et al., 2022). Specifically,

$$H = 2c_p M_{air} g_{bH} (T_L - T_A) \text{ [W m}^{-2}\text{]}, \quad (7)$$

where M_{air} is the molar mass of air and g_{bH} is boundary layer conductance to heat transfer. The flux is doubled because both sides of the leaf participate in heat transfer. The conductance g_{bH} is

414 in turn a function of wind speed (u) measured at a given layer, the characteristic leaf dimension
415 (d, set to 0.01 m in all sites), and the molar density of air (ρ_{mol}):

$$g_{bH} = 0.006\rho_{mol}\frac{u^{0.6}}{d^{0.4}}\ [\text{mol m}^{-2}\ \text{s}^{-1}]. \quad (8)$$

416 2.7 Model assessment

417 We assessed our model's performance by comparing modeled leaf temperature with
418 radiometer T_{bio}. We emphasize that since T_{bio} exhibits bias, this exercise does not suffice to
419 validate our model. However, in the absence of a suitable validation dataset, this exercise helps
420 us understand potential bias in model output. Since model layers did not necessarily collocate
421 with radiometers, we paired each model layer with the nearest radiometer in the canopy. If more
422 than one model layer corresponded to the same radiometer, we used the average model leaf
423 temperature across all corresponding layers for model assessment (Figure S4).

424 2.8 Leaf thermoregulation

425 We employed several analyses to quantify aspects of leaf thermoregulation. To answer
426 our first research question, we calculated the proportion of periods where $T_L < T_A$ as well as
427 whether the model II regression slope of T_L on T_A was smaller than one across canopy layers. To
428 answer our second research question, we calculated the non-transpiring leaf temperature in the 3-
429 T method by re-running our model with $g_s = 0$. In that scenario, absorbed radiation is only
430 dissipated by sensible heat transfer. We ran both the standard model and the model with $g_s = 0$
431 across all canopy layers to examine how the thermal regimes of evergreen forests varied as a
432 function of height in the canopy, microclimate, and forest site characteristics.
433 To evaluate the effect of water availability on leaf thermal regime, we used mixed effects
434 modeling as implemented in the R package lme4 (Bates et al., 2015). After Guo et al. (2023b),

435 we quantified water availability as the ratio of evapotranspiration to potential evapotranspiration
436 (f_{ET}) between 10:00 and 14:00 local time. We then fit two models with mean midday T_L across
437 all canopy layers as the response variable (Table S2). In the first model, T_L was solely a function
438 of T_A, which was a random effect across sites. This base model is essentially equivalent to
439 calculating β across all sites. In the second model, we added an interaction term between T_A and
440 f_{ET} as an additional random effect. We evaluated the significance of the interaction term with a
441 likelihood ratio test and reported the effective leaf-air temperature slope under water-limited
442 conditions ($f_{ET} = 0$) and well-watered conditions ($f_{ET} = 1$).

3 Results

3.1 Comparison with T_{bio}

Model leaf temperature was well-correlated with T_{bio} in all sites (

Table 2; $R^2 \geq 0.70$ in all cases). We note that R^2 is the best measure of model performance in Table 2 because bias in T_{bio} would distort model performance measures based on absolute difference. In ABBY, DEJU, JERC, and WREF, modeled leaf temperature showed little bias when compared to T_{bio}. By contrast, in OSBS, RMNP, and TALL, our model systematically predicted that leaves were cooler than T_{bio}. This cold bias became more pronounced when T_{bio} exceeded 35 °C (Figure 3). Given that non-leaf background is typically warmer than leaves, the cold bias in our model was consistent with modeling realistic leaf temperatures. Model bias was unrelated to site LAI since our model showed the warmest bias at DEJU and WREF, which had the lowest and highest LAI, respectively.

Table 2: Leaf temperature model validation statistics derived from the comparisons shown in Figure 3. RMSE: root mean square error. R^2: proportion of variance explained.

Site	RMSE (K)	Bias (K)	R^2
ABBY	2.14	0.38	0.91
DEJU	2.19	0.12	0.82
JERC	1.31	-0.51	0.86
OSBS	4.07	-3.06	0.72
RMNP	6.10	-3.33	0.72
TALL	3.22	-2.69	0.85
WREF	1.87	0.69	0.93

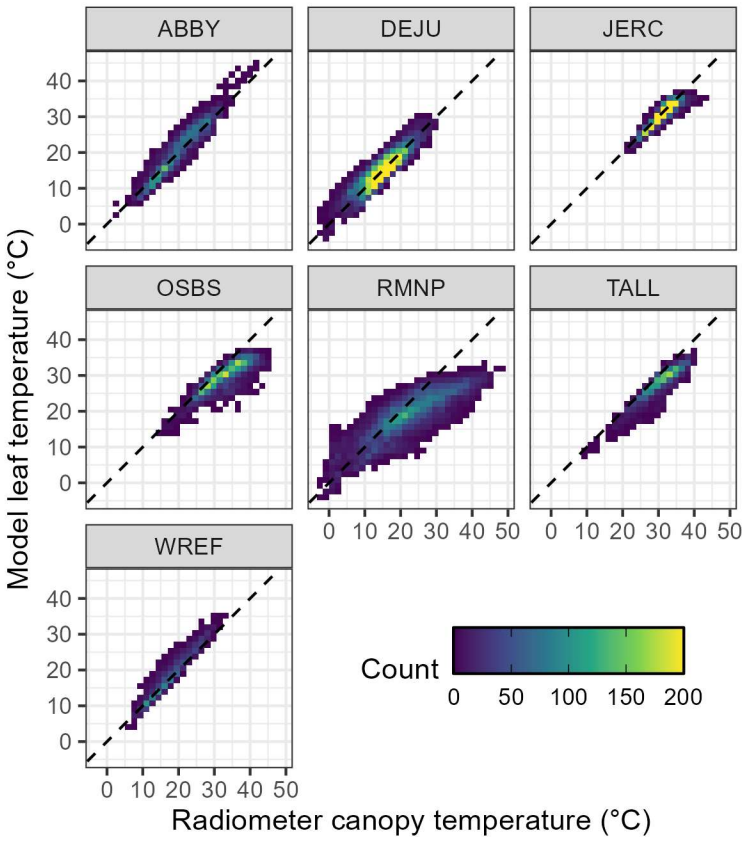

458

459 Figure 3: Comparison between T_{bio} and our modeled leaf temperature. Results from all layer-
460 radiometer pairings are shown together. Dashed line in each panel is 1:1.

461 3.2 Leaf temperature slopes and forcings

462 Modeled leaf temperatures were inconsistent with the limited homeothermy hypothesis.
463 No leaf-air temperature regression slopes were smaller than one across all sites and model layers
464 (Figure 4). Throughout the canopy in all sites except WREF, leaves warmed faster than air. At
465 WREF, upper-canopy leaves warmed faster than air, but lower- and middle-canopy leaves
466 remained close to air temperature. Throughout the day, leaf-air temperature slopes rose in the
467 morning and fell in the afternoon (Figure S5). This result is consistent with the diurnal hysteresis
468 in T_L documented in Still et al. (2022). Periods with modeled $T_L < T_A$ were less common in the
469 lower canopy than in the upper canopy in all sites except for WREF. In DEJU, which had the

greatest proportion of periods with modeled $T_L < T_A$, upper-canopy leaves were cooler than air only about a tenth of the time. Leaves were typically cooler than air in the late afternoon, and such periods were more common towards the end of the growing season (Figure S6).

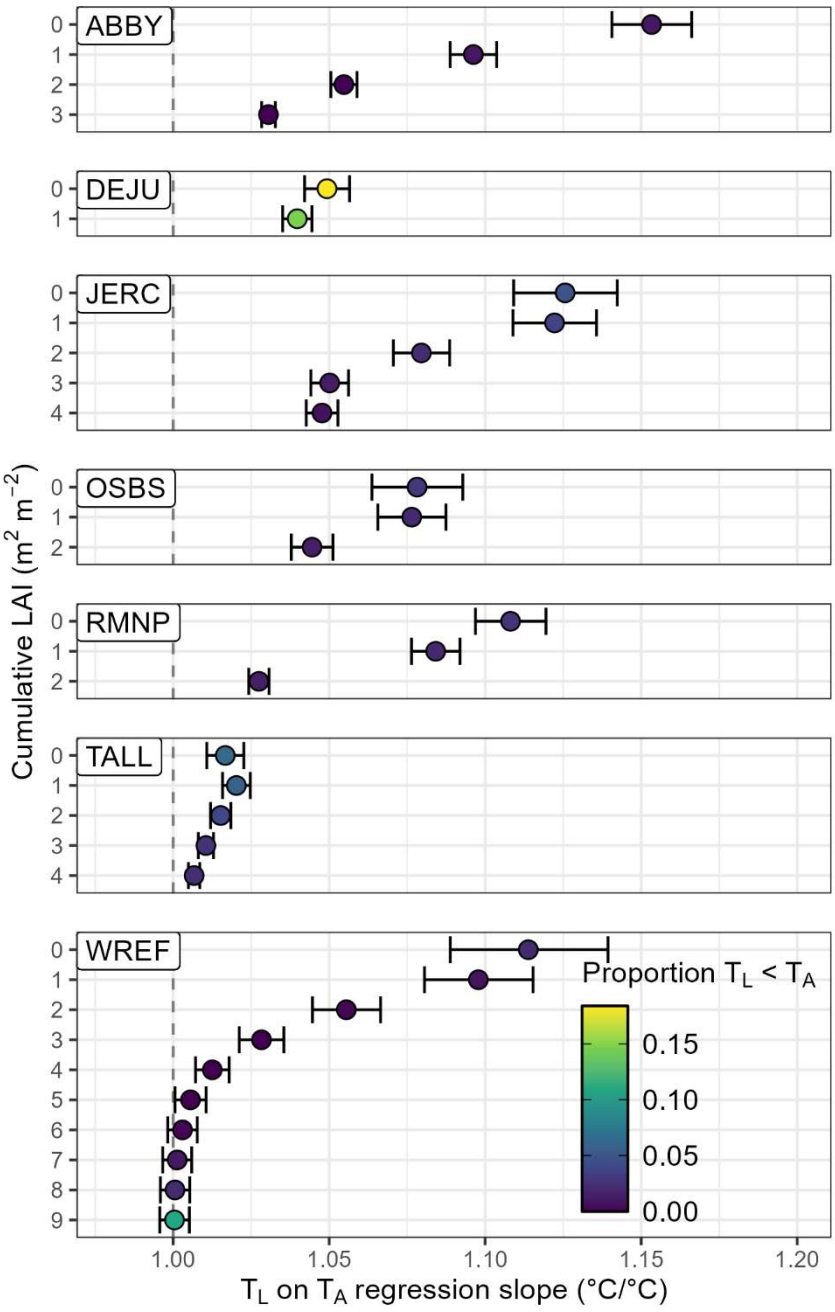

Figure 4: Results of model II linear regressions of T_L as a function of T_A across all forest sites in the analysis. Error bars are the 95% confidence interval of the regression slope. Points are

colored by the proportion of instances where $T_L < T_A$. Vertical dashed line demarcates a slope of one.

There were a minority of cases where $T_L < T_A$ and we sought to determine which of the fluxes in Eq. (1) produced these cases. Since H has the opposite sign and is proportional to $T_L - T_A$, this flux warms the leaf when $T_L < T_A$ and can be ruled out. Comparing R_n and λE, we find that evaporative cooling was actually higher among warmer-than-air leaves than among cooler-than-air leaves (Figure 5). If limited homeothermy is correct, we would expect the opposite to be true. High R_n was necessary to support evaporative cooling, but the warming effect of radiation was stronger than evaporative cooling. This pattern indicated that $T_L < T_A$ only when leaves had a reduced radiation load such that leaf blackbody radiance was sufficient to cool the leaf below air temperature.

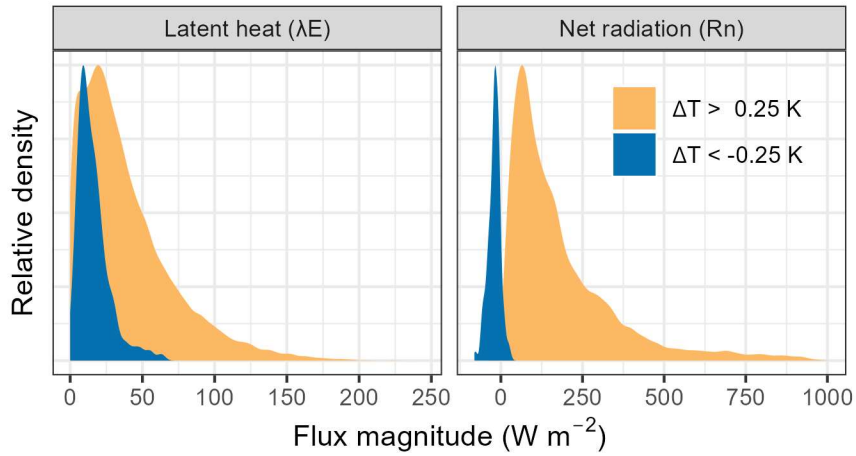

Figure 5: Relative density of latent heat and net radiation flux for leaves at least 0.25 K warmer or cooler than air. Note that sign conventions follow Eq. (1) positive latent heat flux indicates a cooling effect, while positive net radiation indicates a warming effect.

Given that our model underestimated GPP in comparison to another model from He et al. (2018) (Figure S7), we were concerned that our it overpredicted lower-canopy leaf temperature by underestimating the latent heat flux from transpiration. Therefore, we conducted a sensitivity analysis of leaf-air temperature slopes with respect to the parameter g_1 in WREF. Since g_1 is

inversely related to water-use efficiency, plants use more water as g_1 increases. So, manipulating g_1 simulated the effect of increased canopy transpiration on leaf temperature.

We found that the absence of limited homeothermy throughout the canopy was robust to uncertainty in g_1. Increasing g_1 from 1 to 9 at WREF (the fitted value was 1.23), causing stomatal conductance to be modified by a factor of six and led to more incidences of $T_L < T_A$, but the leaf-air temperature slope remained near to or larger than one (Figure S8). Therefore, despite multiplying the stomatal conductance of the canopy by a factor of six at WREF, all canopy layers warmed at the same rate or even faster than air.

Water availability modified the leaf-air temperature slope across all sites. We found that midday mean ΔT was negatively correlated with water availability across all sites except JERC and TALL, where the relationship was nearly flat (Figure S9). With mixed effects models, we found that adding an interaction term between T_A and f_{ET} improved goodness-of-fit ($\chi^2 = 290.55$; $\mathrm{df} = 2; p < 2 \times 10^{-16}$). Random effects in the more complex model indicate that under dry conditions ($f_{ET} = 0$), the leaf-air temperature slope is larger than one, but under wet conditions ($f_{ET} = 1$), the leaf-air temperature slope can be near or slightly smaller than one (Table S3).

Leaf temperature forcings derived with the 3-T method also showed little evidence for limited homeothermy. If limited homeothermy is correct, we would expect cooling from transpiration to have a greater magnitude and exhibit more variability than warming from radiation. Instead, leaf temperature forcing from absorbed radiation was larger and more variable than cooling from transpiration across all sites and vertical layers (Figure 6). Moving lower in the canopy, both forcings became smaller. This trend reflected two effects of shortwave light attenuation in the canopy. Heating from downwelling shortwave radiation was lost, leaving only

518 the longwave flux from the surrounding air and foliage to heat leaves. Simultaneously, less

519 shortwave radiation reduced the amount of energy available for photosynthesis and transpiration.

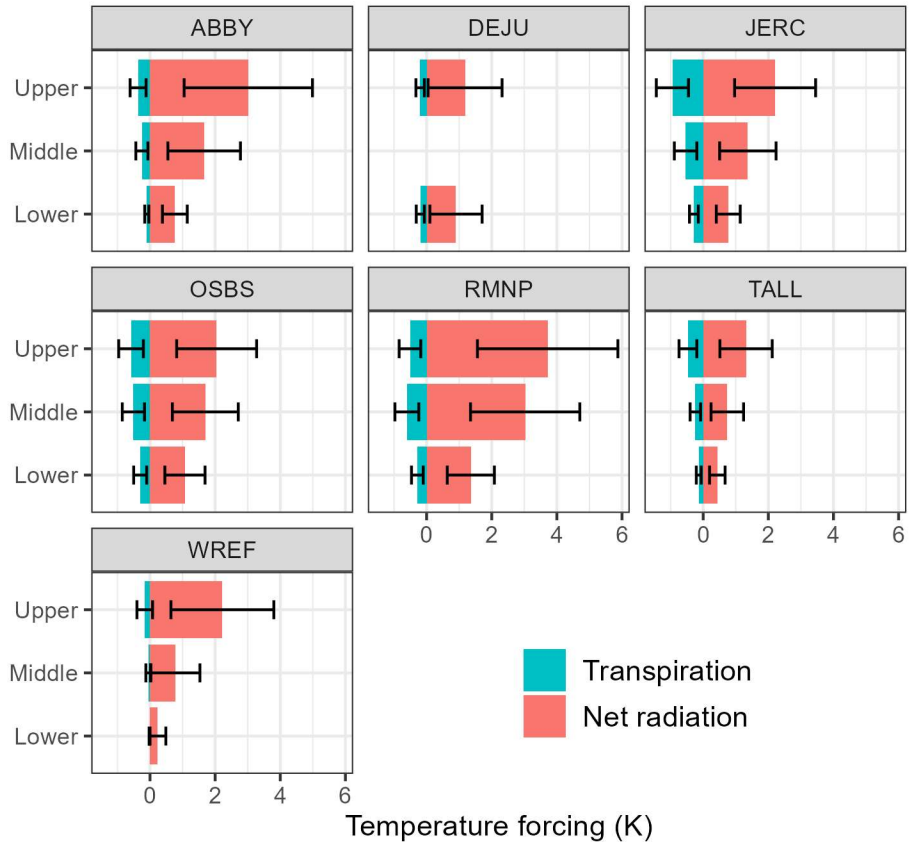

520

521 Figure 6: Mean leaf temperature forcing from transpiration and net radiation. Here, "Upper,"
522 "Middle," and "Lower" refer to canopy sections. The upper canopy is the model layer at the
523 canopy top, the lower canopy is the lowest model layer, and the middle canopy is all other model
524 layers pooled together. DEJU does not have a middle canopy because only two layers were
525 included there. Forcings were derived by comparing model output with a non-transpiring leaf
526 temperature (T_{NT}) where stomatal conductance and thus the latent heat flux was set to zero. Net
527 radiation forcing is equal to $T_{NT} - T_A$, while transpiration forcing is equal to $T_L - T_{NT}$. Error bars
528 show one standard deviation about the mean.

529 3.3 Leaf conductance sensitivity analysis

530 Comparing the three fluxes in Eq. (1) reveals that leaves were consistently coupled with

531 the surrounding air. Of the three fluxes, R_n and H were consistently larger than λE across all

532 vertical positions (Figure S10). Such rapid sensible heat transfer is also reflected in the leaf-air

decoupling coefficient, which was closer to zero than one across all sites and vertical positions (Figure S11).

Blonder and Michaletz (2018) found that both stomatal conductance and boundary layer conductance to heat transfer must be high for leaves to be cooler than air at steady state. Here, we found that the interplay between stomatal and boundary layer conductance depended on radiation load, which in turn drives key variables in our model like air temperature and vapor pressure deficit (Figure 7). Boundary layer heat conductance was typically an order of magnitude larger than stomatal conductance, which drove substantial changes in leaf temperature only when the radiation load was extremely high (800 W m^{-2}) or low (400 W m^{-2}). Under a typical radiation load, leaf temperature varied by less than 1 K over the entire range of stomatal and boundary layer heat conductance values considered.

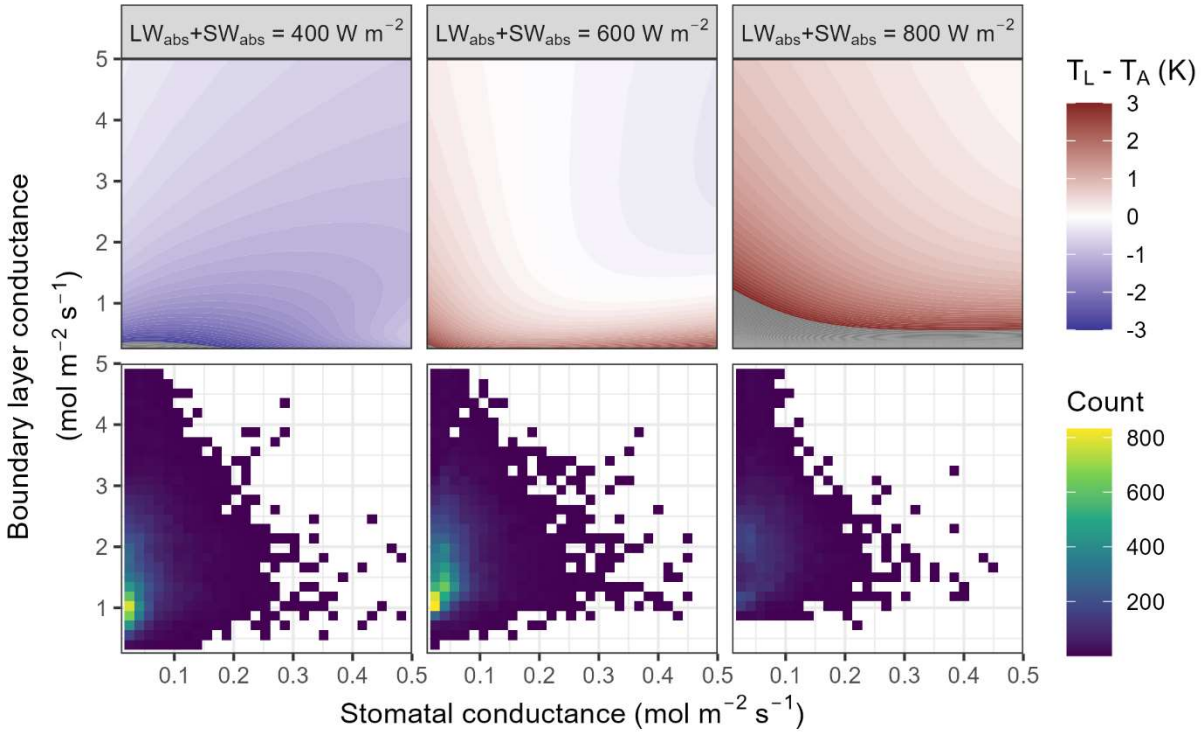

Figure 7: Leaf temperature depends on the interplay of radiation load, stomatal conductance, and boundary layer heat conductance. Top row: shaded regions describe leaf-air temperature

difference under the following hypothetical conditions: air temperature 20 °C, air pressure 100 kPa, relative humidity 50%, leaf emissivity 0.95, leaf shortwave absorptivity 0.50, and radiation load as provided in facet titles. Note that since radiation loads are fixed in this exercise, data in the top row are independent of model layer. Gray regions are outside the color range. Bottom row: distribution of modeled stomatal and boundary layer conductance at the corresponding radiation load across our study sites.

4 Discussion

Limited homeothermy was no more likely to occur in lower-canopy foliage than in upper-canopy foliage in our model. We attribute this result to high boundary layer conductance in needle-shaped leaves that tightly coupled leaf temperature to surrounding air and the use of sensible heat transfer to dissipate absorbed radiation (Figure S10). From Eq. (1), absorbed radiation warms the leaf while latent heat cools the leaf. The difference between R_n and λE is accounted for by H, whose sign always opposes the leaf-air temperature difference as in Eq. (3). When R_n is larger than the sum of H and λE, $T_L > T_A$, and by definition H is positive (i.e., sensible heat flows out of the leaf). Conversely, if R_n is smaller than λE, $T_L < T_A$ and H becomes negative (i.e., sensible heat flows into the leaf). In both cases, high boundary layer conductance supports rapid sensible heat transfer that couples leaf and air temperature.

Our modeling results were consistent with sensible heat transfer coupling leaves and air. When leaves absorbed more radiation in the upper canopy, sensible heat flux also increased while latent heat flux showed slight change (Figure S10). Rapid sensible heat transfer requires a high boundary layer conductance, which we modeled as a decoupling coefficient near zero (Figure S11). For leaf temperature to deviate from air temperature under strong coupling, a large latent heat flux was necessary to overcome the sensible heat flux. This was never observed at any of the layers at any of our sites. Warming from absorbed radiation was stronger than cooling from latent heat (Figure 6) and thus leaves were consistently warmer than air.

The importance of sensible heat flux signals that leaf shape is critical in determining thermal regime. Ours and previous work suggests that the needle leaf shape serves to offset thermal stress with sensible heat transfer. Indeed, sensible heat flux can be just as large a cooling force as latent heat flux in drought-exposed pine forests (Muller et al., 2021) and in our results

this flux almost always moved heat out of the leaf (Figure S10). However, such strong leaf-air coupling also prevents transpiration cooling even if soil moisture is abundant.

Our model led to a counterintuitive result: higher transpiration was actually associated with leaves that were warmer than air (Figure 5). We interpret this pattern as a consequence of the greater thermal effect of absorbed radiation than transpiration cooling (Figure 6). Absorbed radiation directly warms leaves but has a more complex effect on transpiration. Warming can both enhance transpiration cooling by increasing vapor pressure deficit and diminish transpiration cooling by inducing stomatal closure. These opposing trends dampen the effect of absorbed radiation on transpiration, allowing the direct warming effect to outpace transpiration cooling. Decoupling of photosynthesis and transpiration could allow for increased transpiration under warm conditions, but our model did not capture this effect because we implicitly coupled photosynthesis and transpiration in our estimate of stomatal conductance (Medlyn et al., 2011).

Although we did not find evidence for limited homeothermy in conifer forests, we did find that the leaf-air temperature slope can be less than one when water is abundant (Figure S9; Table S3). This result affirms several recent studies which emphasize the importance of soil moisture in plant thermoregulation (Cook et al., 2021; Posch et al., 2024; Rastogi et al., 2022). We also note that stomatally mediated thermoregulation still plays a role in plant function, even if transpiration is not as strong a cooling force as the limited homeothermy hypothesis suggests. Such forms of thermoregulation include short-term decoupling of transpiration and photosynthesis to avert thermal damage (Marchin et al., 2023) and shorter, less dense needles to support rapid sensible heat transfer (Gauthey et al., 2023). These observations suggest that various forms of thermoregulation can result under extreme circumstances that help mitigate damage but not necessarily to maintain homeostasis as the limited homeothermy hypothesis

suggests. It is also perhaps a misnomer to call these phenomena homeothermy since plants do not directly sense temperature, but instead respond to slight biochemical changes induced by ambient temperature (Ruelland and Zachowski, 2010).

Even if there is consensus on the importance of thermoregulation, significant disagreement over leaf temperature dynamics remains. Studies based on proximal remote sensing of canopy and leaf temperature do not support the limited homeothermy hypothesis (Aubrecht et al., 2016; Kim et al., 2018; Still et al., 2022; Zhou et al., 2023), but studies based on gas-exchange data or global leaf trait data do support the limited homeothermy hypothesis (Blonder and Michaletz, 2018; Michaletz et al., 2016). Large errors in measuring leaf temperature with older gas-exchange instruments have been documented (Garen et al., 2022; Still et al., 2019b), but we suggest that water availability may also underlie this disagreement. The original formulation of the limited homeothermy hypothesis required well-watered conditions (Mahan and Upchurch, 1988) and accompanying observations of limited homeothermy were in irrigated cotton plants (Upchurch and Mahan, 1988). If well-watered conditions are a requirement of limited homeothermy as ours and other recent results suggest (Cook et al., 2021; Posch et al., 2024), then this phenomenon should not be commonly observed across many naturally occurring ecosystems.

For example, we suspect that water availability may have contributed to different thermal regimes reported in Blonder and Michaletz (2018). Three environments are depicted in Figure 1 from that study: subalpine meadows, high deserts, and forests and meadows. The authors state that leaf temperature was measured with thermocouples in intact plants in subalpine meadows and high deserts, while branch cuttings were left to stand in water before measuring leaf temperature with a portable gas-exchange instrument in forests and meadows. We acknowledge

623 that immersing cuttings in water is standard procedure to prevent embolisms when collecting
624 gas-exchange data, but we suspect that this procedure may add a cold bias to leaf temperature
625 measurements. We suppose that leaves had abundant moisture when measured in forests and
626 meadows but were moisture-limited when measured in subalpine meadows and high deserts.
627 Consequently, homeothermic leaves were only observed in forests and meadows. This view is
628 consistent with the requirements for limited homeothermy laid out in Mahan and Upchurch
629 (1988). It is not clear which measurement method was most prevalent in the global leaf trait data
630 used by Michaletz et al. (2016) but measuring leaf temperature on cuttings immersed in water is
631 likely to be a source of a cold bias in leaf temperature data.

632 While our approach is limited by the assumptions regarding leaf angle distribution and
633 leaf responses to photosynthesis, we emphasize that our conclusions are robust to these
634 assumptions. We evaluated our model against measured T_{bio}, which is itself influenced by
635 warmer non-leaf backgrounds. If T_{bio} is not representative of leaf temperature because few
636 leaves are in view of a radiometer, then our model predictions should be more representative of
637 actual leaf temperature. If T_{bio} is representative of leaf temperature, then our inferred cold bias
638 would make us more likely to erroneously conclude that limited homeothermy occurs. Instead,
639 we concluded that limited homeothermy does not occur. Therefore, it is unlikely that our
640 conclusion on limited homeothermy arose from model bias.

641 Nonetheless, our approach is not without caveats. We found that our model predicted a
642 lower proportion of GPP attributed to shade leaves as compared to a similar modeling study
643 performed by He et al. (2018), particularly in forests with low LAI (Figure S7). We reiterate that
644 total canopy GPP in our model was forced to equal that estimated from eddy covariance. That is,

our possible underestimation of shade GPP does not reflect underestimation of total GPP, but a misallocation of GPP to sunlit over shaded leaves.

Our study and previous work make clear that leaf temperature is usually warmer than air temperature in forest ecosystems that have been studied. Satellite remote sensing confirms our canopy-scale study; the majority of leaf-on-air temperature slopes on Earth are near or above 1, but can be as low as 0.75 (Guo et al., 2023a). We suggest that future research on leaf temperature should shift away from describing the decoupling of leaf and air temperatures and toward analyzing the implications of leaves decoupled from air. Two broad directions are feasible: prediction of future ecosystem function and development of monitoring tools based on forest canopy temperature.

Prediction of future ecosystem services entails using existing thermal data to parameterize models of forests in a warming world. Rising temperatures and drought stress in forests may reduce carbon sequestration (Chen et al., 2024), increase the risk of drought-induced mortality (Anderegg et al., 2013; Marchin et al., 2022), or damage foliage from extreme heat (Still et al., 2023b). Leaves warming faster than air would mean that evaporative demand at leaf stomata will increase faster than climate models suggest and that leaf thermal thresholds will be reached sooner. However, it is unclear to what extent carbon sequestration or tree mortality could be affected by changes in leaf thermal regimes. Understanding how decoupling of leaf and air temperature will push forests closer to critical thermal thresholds (Doughty et al., 2023) or accelerate the conversion of forests to non-forests (Coop et al., 2020) is a prospect for future research.

Parallel research in crop science implies that canopy temperature could be a useful tool to monitor forest health. The crop water stress index (Idso et al., 1981) has been used for decades to

668 monitor drought stress and identify disease in agricultural settings. Similar applications in forests
669 are less common, but early work suggests that anomalous tree canopy temperature is indicative
670 of stress, either from drought (Smigaj et al., 2017) or bark beetle infestation (Sprintsin et al.,
671 2011; Zakrzewska and Kopeć, 2022). The advent of high-resolution thermal remote sensing
672 platforms, such as ECOSTRESS (Fisher et al., 2020) and the forthcoming SBG-TIR mission
673 (Cawse-Nicholson et al., 2021) offer abundant opportunity for thermal monitoring in forest
674 ecosystems.

675 Our conclusion that evergreen needleleaf temperature is similar throughout the canopy
676 and primarily forced by absorbed radiation encourages empirical pursuit of such questions in
677 both conifer and broadleaf forest ecosystems. Similarity between upper and lower-canopy
678 thermal regimes means that remote sensing of thermal stress in the canopy top may also be
679 indicative of thermal stress lower in the canopy. Also, our modeling suggests that leaf
680 microclimate and radiation load drives most of the variation in leaf temperature (Figure 7), with
681 water availability modulating this relationship (Figure S9; Table S3). The fact that conifer leaf
682 temperatures are primarily a function of environmental conditions, and not transpiration, relaxes
683 the need for precise evapotranspiration models to understand leaf temperature.

684 ### 4.1 Conclusions

685 Our energy balance modeling approach adds to the growing body of evidence that limited
686 homeothermy does not occur in evergreen needleleaf forests because of water availability
687 limiting the effectiveness of evaporative cooling. Across all canopy layers and sites, leaves
688 warmed faster than air and leaf temperature forcing was stronger from warming due to radiation
689 absorbed from the environment rather than cooling from transpiration. In the few instances when
690 $T_L < T_A$, this was caused by negative R_n, rather than large positive λE. However, when

691 evapotranspiration is especially high, the leaf-air temperature slope can approach or be less than
692 one. Although our modeled leaf temperature exhibited cold bias in comparison to T_{bio}, our
693 results were robust to changes in key model parameters. These results suggest that the thermal
694 regime of conifer forests is governed by physical constraints that transpiration cooling cannot
695 overcome.
696

Declaration of Competing Interests

None.

Data Availability Statement

Code used to download data, run the model, and generate the figures in this manuscript is available under the MIT license at https://github.com/s-kganz/LeafTemperature.

Acknowledgements

This material is based upon work supported by the National Science Foundation Graduate Research Fellowship Program under Grant No. DGE-2140004. Field work and computational needs were supported by the Precision Forestry Cooperative at the University of Washington. We thank Christian Torgersen and David Butman for helpful comments on earlier versions of this manuscript. We thank Anthony Stewart and Rachel Deininger (UW RSGAL) for collecting the lidar point clouds from which the ABBY, DEJU, and RMNP tree graphics in Figure 1 were derived.

The National Ecological Observatory Network is a program sponsored by the National Science Foundation and operated under cooperative agreement by Battelle. This material is based in part upon work supported by the National Science Foundation through the NEON Program. Funding for the Ameriflux data portal was provided by the U.S. Department of Energy Office of Science. Specific acknowledgement of Ameriflux and NEON data products is provided in Supplementary Information.

Supplementary Information

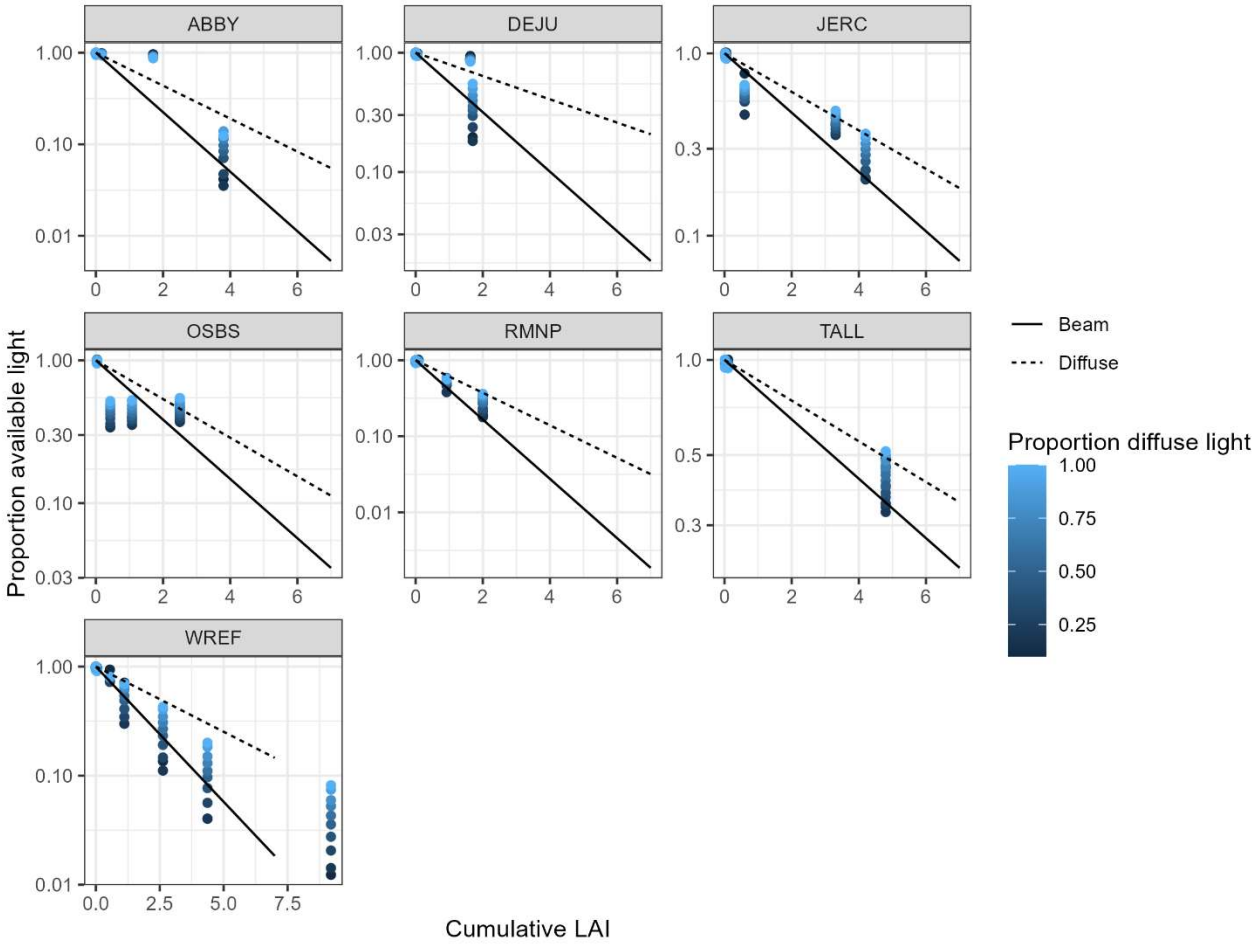

Figure S1: Fit results of our modified Beer-Lambert relationship for light attenuation. Each point shows the geometric mean proportion of light transmitted from the top of the canopy, colored by the proportion of diffuse light at the top of the canopy. Lines show the fit results for endpoints where top-of-canopy light is entirely beam or entirely diffuse. In all sites, diffuse light penetrated the canopy more effectively than beam light.

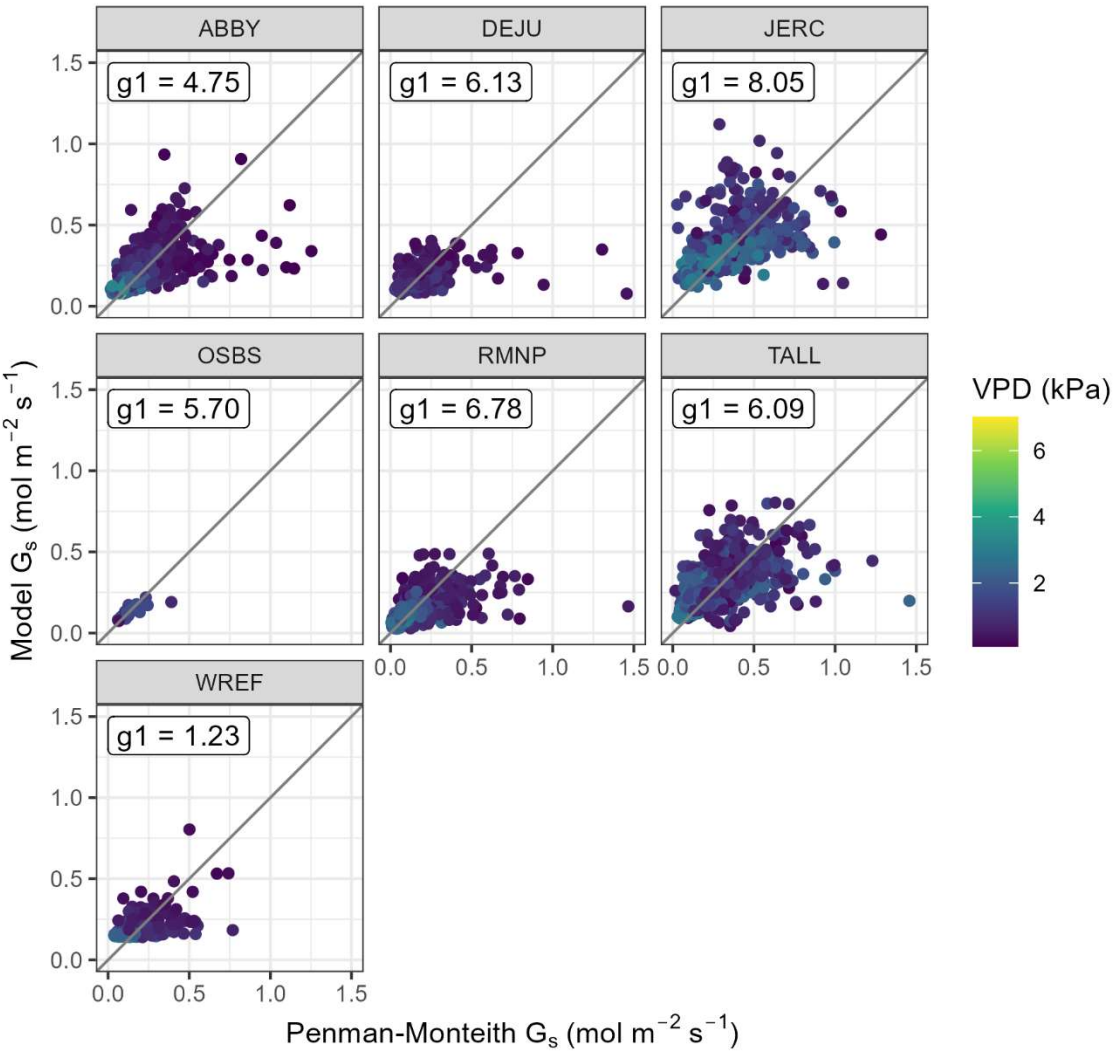

725

726 Figure S2: Results of our fitting stomatal conductance model parameters to canopy-scale carbon
727 and water fluxes. Canopy conductance (G_s) was derived either by inversion of the Penman-
728 Monteith equation with canopy-scale fluxes or with a generalized Medlyn model (Li et al.,
729 2019). Fitted values for g_1 are annotated on each panel, and gray lines are 1:1.

730

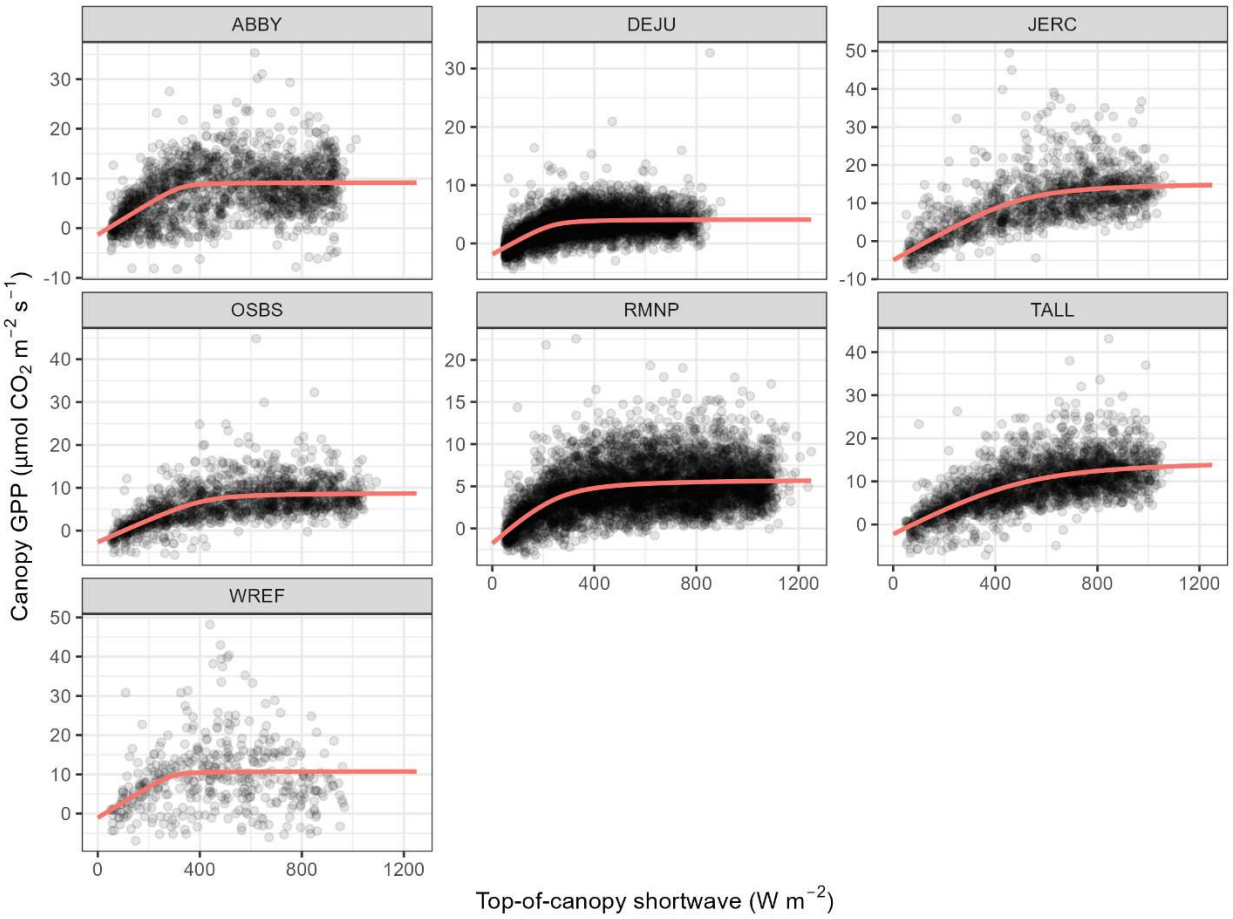

731

732 Figure S3: Photosynthesis-light response curves. Red lines show the fit result, while points show
733 data. Each fit was made with the photosynthesis R package using the curve parameterization in
734 Marshall and Biscoe (1980).

735

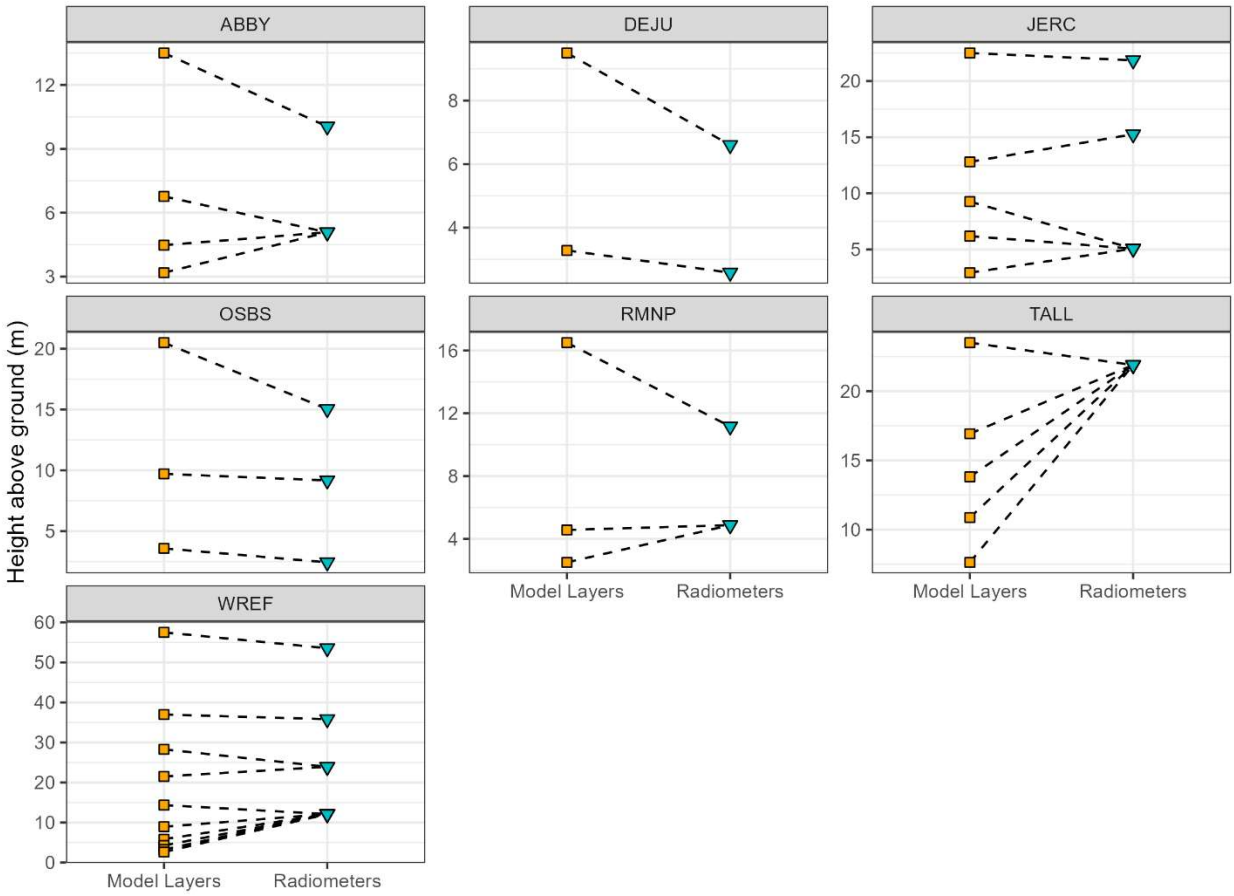

Figure S4: Paired model layers and canopy radiometers for model validation. Dashed lines indicate which model layers were compared with which canopy radiometers. If multiple model layers corresponded to the same radiometer, the average leaf temperature across all layers was compared with radiometer biological temperature.

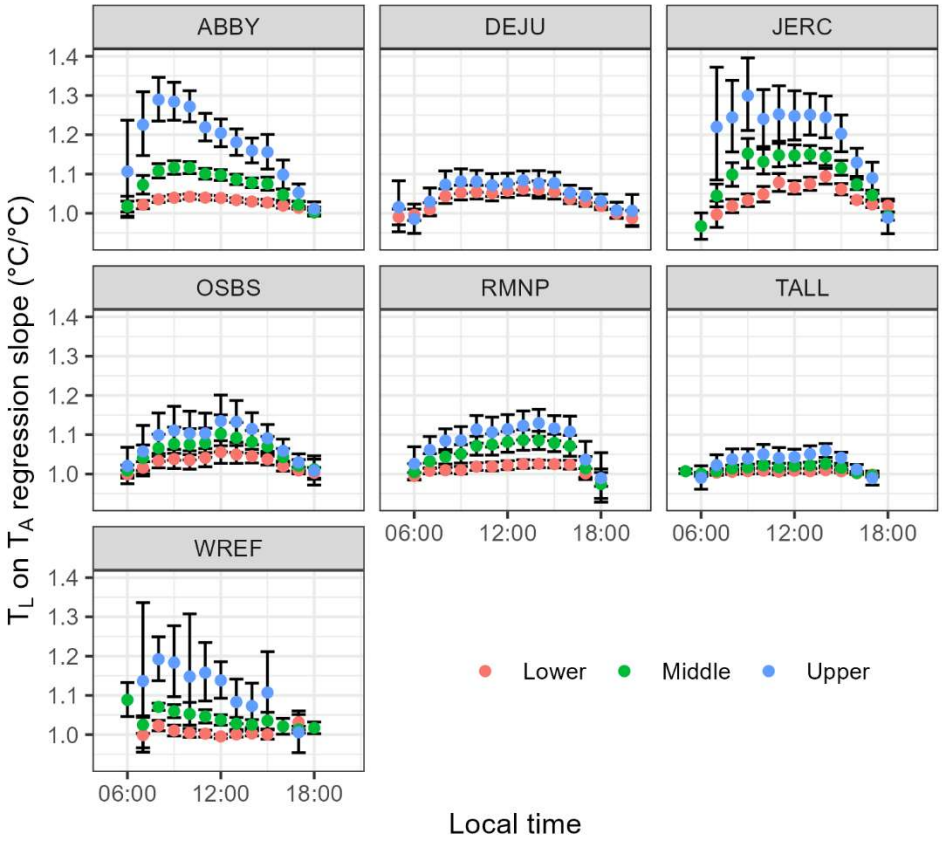

742

743 Figure S5: Diurnal patterns in the regression slope between leaf and air temperature. Points and
744 error bars are as in Figure 4, and canopy strata are categorized as in Figure 6.

745

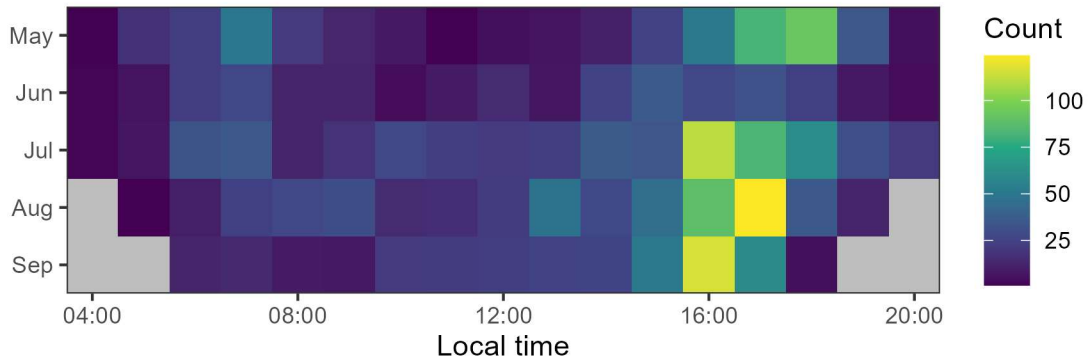

746

747 Figure S6: Seasonal and diurnal distribution of periods where modeled $T_L < T_A$. All sites are
748 combined in this figure. Gray cells indicate periods where no modeling occurred due to a lack of
749 sunlight in all sites.

750

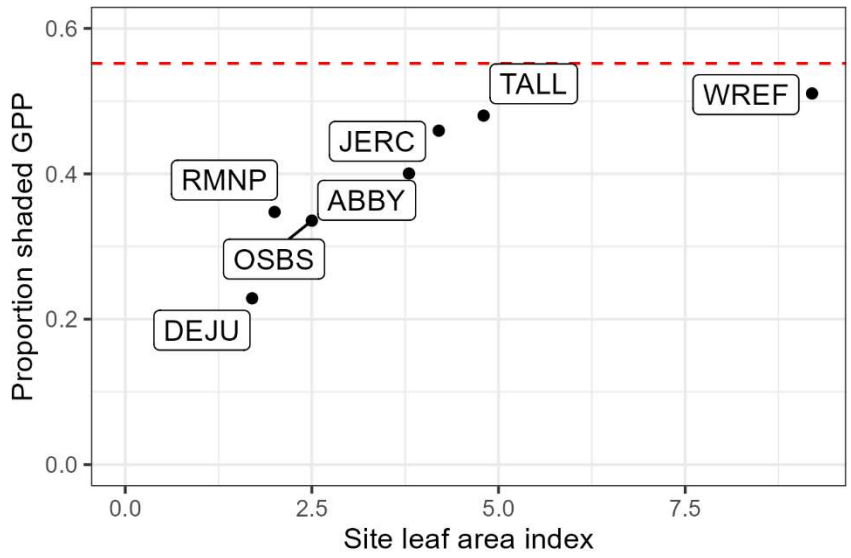

Figure S7: Proportion of gross primary production (GPP) attributed to shaded leaves. We estimated shade GPP from the proportion of shaded leaves in each model layer using Eq. (C4) in Wang and Leuning (1998). For example, if Eq. (C4) predicted that a layer was 50% shade leaves, we assumed that 50% of layer photosynthesis was due to shade leaves. Then, we summed shade photosynthesis across all layers and timesteps for each site and calculated shade GPP as the ratio of this sum to total site GPP. Modeled shade GPP (dots) consistently underestimated mean shade GPP for evergreen needleleaf forests (horizontal red line) calculated by He et al. (2018) and was positively correlated with site LAI ($r = 0.82$).

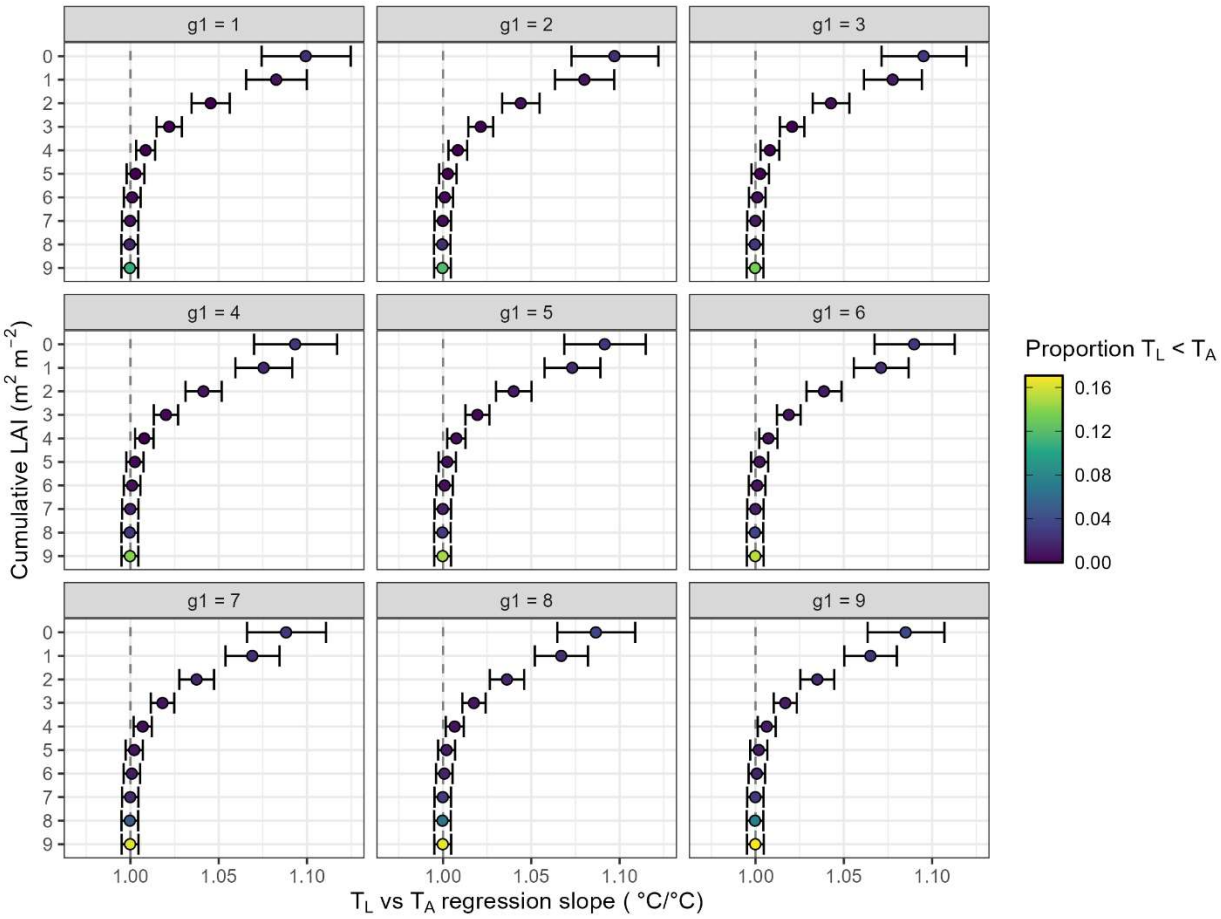

762

763 Figure S8: Sensitivity analysis of leaf-on-air regression slopes with differing optimal stomatal
764 model g_1 values at WREF. Regression slopes were insensitive to the value of g_1 across all model
765 layers. As g_1 increased from 1 to 9, leaf-on-air regression slopes did not change, but $T_L < T_A$ was
766 predicted more often in the upper canopy. The default value for g1 was set to 1.23 based on our
767 model calibration procedure.

768

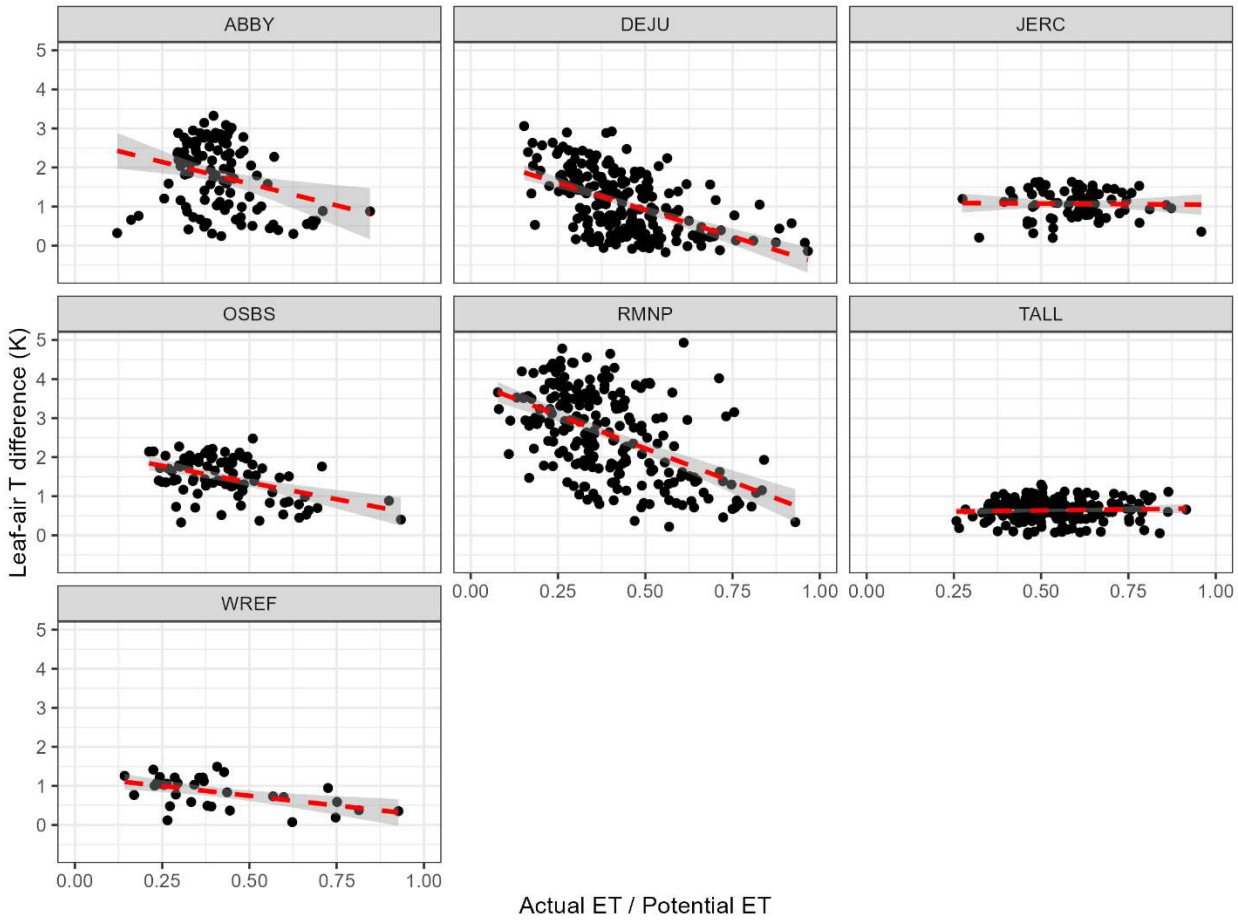

Figure S9: Relationship between ΔT and water availability expressed as the ratio between actual and potential evapotranspiration. Data shown are daily means between 10:00 and 14:00 local time. Potential evapotranspiration was calculated with top-of-canopy radiation flux and meteorology with the R package bigleaf. Dashed red lines show linear fit and shading shows 95% confidence interval. Note that 10 data points with AET / PET > 1 are excluded from the panel for DEJU.

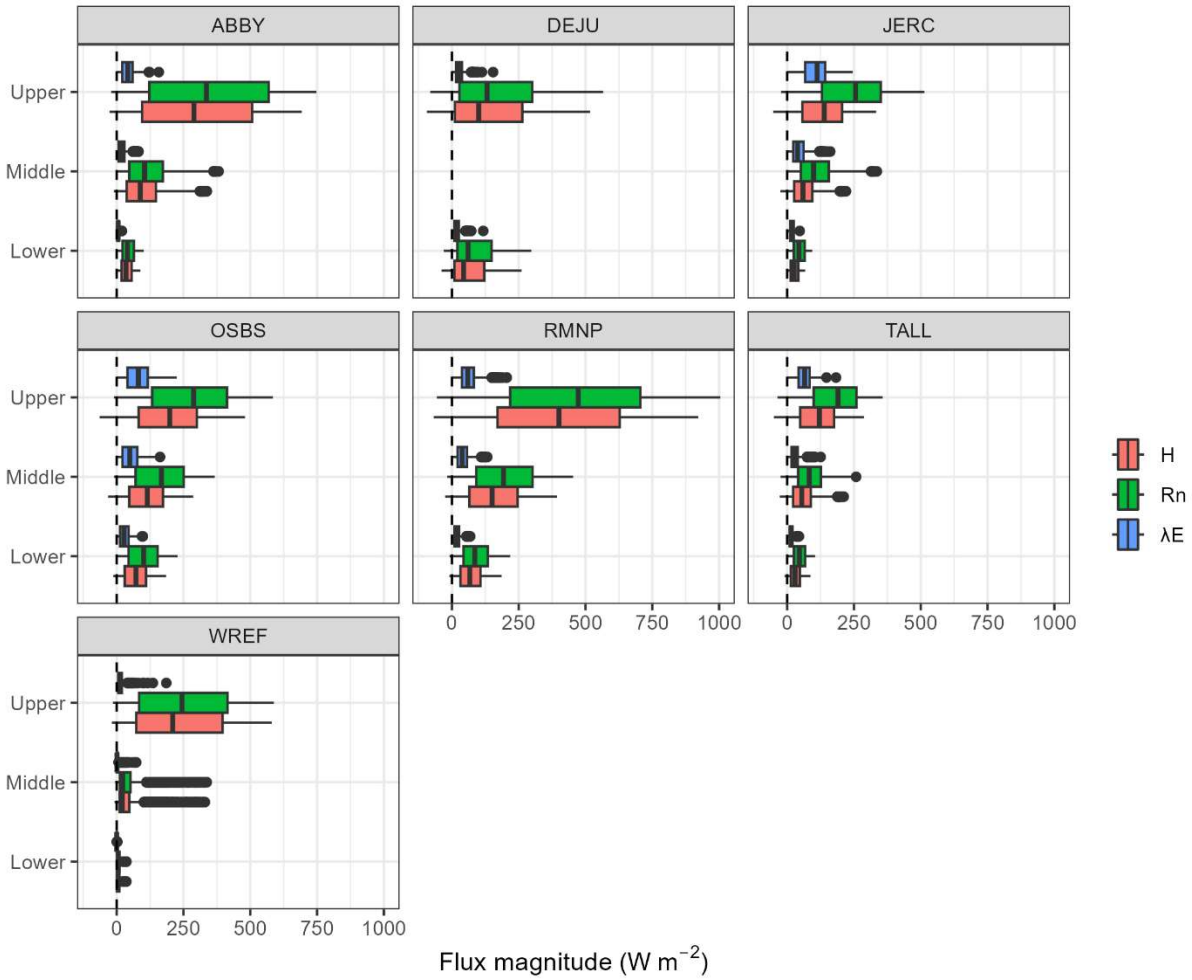

Figure S10: Boxplots of sensible heat, net radiation, and latent heat flux across sites and canopy positions. Sign conventions are as in Eq. (1). That is, positive sensible heat and latent heat flux indicate a cooling effect, while a positive net radiation flux indicates a warming effect. Canopy positions are as in Figure 6, and the dashed line in each panel indicates zero flux.

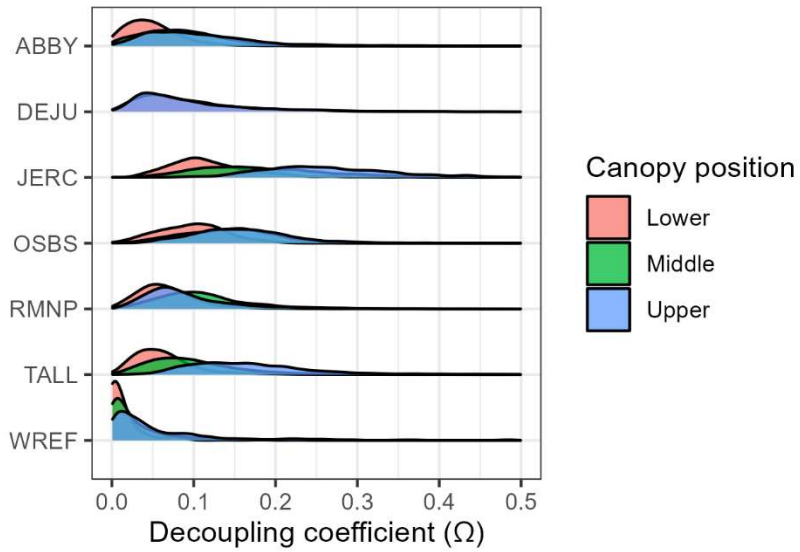

784

785 Figure S11: Relative density of the leaf-air decoupling coefficient across sites and canopy
786 positions. Canopy positions are as in Figure 6.

787

Leaf stomatal conductance example calculation

Consider a hypothetical four-layer forest canopy with light availability as in the table below. These values are for the sake of demonstrating the calculation and do not correspond to measured data. Partitioned eddy covariance data indicate that whole-canopy gross primary production is 5.0 μmol CO_2 m^{-2} s^{-1} while microclimate sensors indicate that vapor pressure deficit is 2.0 kPa, air temperature is 25 °C, and ambient CO_2 concentration is 400 ppm throughout the canopy. Assume that $g_1 = 4.0$ and $m = 0.5$ in the stomatal conductance model and that the light response curve for this canopy is given by $A_{sat} = 6.46$ μmol CO_2 m^{-2} s^{-1}, $\phi_J = 0.017$ μmol CO_2 W^{-1}, $\theta_J = 0.99$.

Canopy Layer	Cumulative LAI (m^2 m^{-2})	Downwelling shortwave radiation (W m^{-2})
1	0	800
2	1	400
3	2	200
4	3	100

Calculations to determine leaf stomatal conductance in each layer are shown in the table below. First, calculate the photosynthesis rate predicted by the light response curve, then normalize this column so that it sums to 1. Then, multiply the normalized photosynthesis rate by the gross primary production rate indicated by eddy covariance data. Finally, use Eq. (6) to calculate leaf stomatal conductance.

Canopy layer	Light response curve photosynthesis rate (μmol CO_2 m^{-2} s^{-1})	Normalized photosynthesis rate (-)	Leaf gross photosynthesis rate (μmol CO_2 m^{-2} s^{-1})	Leaf stomatal conductance (mmol m^{-2} s^{-1})
1	6.40	0.37	1.83	17.5
2	6.01	0.34	1.72	16.4
3	3.36	0.19	0.96	9.2
4	1.69	0.10	0.48	4.6

From this analysis, we find that layer 2 has a similar stomatal conductance as layer 1 despite receiving half as much shortwave radiation.

Calculating leaf coupling and latent heat flux

Our approach to calculating leaf coupling and latent heat flux comes from Jarvin and McNoughton (1986), and additional instructions on these calculations are available in Monteith and Unsworth (2013) and Still et al. (2022). In this approach, total latent heat flux (λE) is the sum of equilibrium latent heat (λE_{eq}) and stomatally imposed latent heat (λE_{imp}) weighted by the leaf-air decoupling coefficient (Ω) that ranges from 0 – 1. We have

$$\Omega = \frac{\epsilon + 1}{\epsilon + 1 + {g_{bH}}/{g_s}} \; [-]$$

where

$$\epsilon = \frac{\partial e_{sat}}{\partial T_a} \times \frac{1}{\gamma} \; [-].$$

We calculated the partial derivative from Tetens' formula and γ is the psychrometer constant for a given air pressure. The latent heat endpoints are

$$\lambda E_{imp} = \lambda g_{tot} \frac{VPD}{P_a} [\mathrm{W\ m^{-2}}]$$

where P_a is air pressure, and λ is the latent heat of vaporization of water. The other endpoint is

$$\lambda E_{eq} = \frac{R_n \epsilon}{\epsilon + 1 + {g_R}/{g_{bH}}} \; [\mathrm{W\ m^{-2}}]$$

where R_n is as in Eq. (2). The conductance g_{tot} is the total leaf conductance to water vapor. We calculated g_{tot} as the serial sum of g_s and g_{bH}, assuming boundary layer conductance to water vapor is 1.08 times that to heat:

$$g_{tot} = \frac{1}{(g_s^{-1} + (1.08 g_{bH})^{-1})} \; [\mathrm{mol\ m^{-2} s^{-1}}].$$

825 The conductance g_R is conductance to radiative heat transfer, which we calculated as

826 $$g_R = 2\rho_{mol}\frac{4\epsilon_f \sigma T_A^3}{\rho_{mass} c_p}\ [\text{mol m}^{-2}\text{s}^{-1}].$$

827 Note that g_R depends on dry air density on a molar basis (ρ_{mol}, mol m^{-3}) and on a mass basis
828 (ρ_{mass}, kg m^{-3}). Multiplying by ρ_{mol} ensures consistent units among all conductances in our
829 calculations.

830

Table S1: List of symbols.

Category	Symbol	Description	Value	Unit
Physical constants	c_p	Heat capacity of dry air.	1,010	J kg^{-1} K^{-1}
	M_{air}	Molar mass of dry air.	0.029	kg mol^{-1}
	σ	Stefan-Boltzmann constant.	5.67 x 10^{-8}	W m^{-2} K^{-4}
	λ	Heat of vaporization of water.	44.2 x 10^3	J mol^{-1}
Microclimate	T_A	Air temperature.	-	K
	P_a	Air pressure.	-	kPa
	γ	Psychrometric constant.	-	kPa K^{-1}
	e_{sat}	Saturation vapor pressure.	-	kPa
	ρ_{mol}	Dry air molar density.	-	mol m^{-3}
	ρ_{mass}	Dry air mass density.	-	kg m^{-3}
	u	Wind speed.	-	m s^{-1}
	VPD	Vapor pressure deficit.	-	kPa
	$[CO_2]$	Ambient CO_2 concentration.	-	ppm
	SW_z	Downwelling shortwave radiation at cumulative leaf area index z.	-	W m^{-2}
	SW_{abs}	Within-canopy absorbed shortwave radiation.	-	W m^{-2}
	LW_{dn}	Within-canopy downwelling longwave radiation.	-	W m^{-2}
Model parameters	z	Cumulative leaf area index, measured from the top of the canopy.	-	m^2 m^{-2}
	d	Characteristic leaf dimension.	0.01	m
	ϵ_f	Leaf emissivity.	0.95	-
	ϵ_s	Soil emissivity.	0.9	-
	s	Leaf scattering coefficient.	0.5	-
	ρ_d	Canopy reflectivity to diffuse shortwave radiation.	0.1	-
	ρ_b	Canopy reflectivity to beam shortwave radiation.	0.1	-
	k_b	Attenuation coefficient for beam radiation in a canopy of black leaves.	-	-
	k_d	Attenuation coefficient for diffuse radiation in a canopy of black leaves.	0.8	-
	k_d^*	Empirical attenuation coefficient for diffuse radiation.	-	-
	k_b^*	Empirical attenuation coefficient for beam radiation.	-	-
	g_1	Conductance model slope parameter.	-	-

Leaf properties	g_0	Conductance model intercept parameter.	-	mol m^{-2} s^{-1}
	m	Conductance model curvature parameter.	-	-
	A_{sat}	Light response curve light-saturated CO_2 assimilation rate.	-	µmol CO_2 m^{-2} s^{-1}
	ϕ_J	Light response curve quantum yield of CO_2 assimilation.	-	µmol CO_2 W^{-1}
	θ_J	Light response curve curvature parameter.	-	-
	T_L	Leaf temperature.	-	K
	ΔT	Leaf-air temperature difference.	-	K
	T_{NT}	Non-transpiring leaf temperature.	-	K
	β	Leaf-on-air temperature regression slope.	-	-
	H	Sensible heat flux.	-	W m^{-2}
	R_n	Net absorbed radiation.	-	W m^{-2}
	λE	Total latent heat flux.	-	W m^{-2}
	λE_{imp}	Latent heat flux, stomatally imposed endpoint.	-	W m^{-2}
	λE_{eq}	Latent heat flux, equilibrium endpoint.	-	W m^{-2}
	g_{bH}	Leaf boundary layer conductance to heat transfer.	-	mol m^{-2} s^{-1}
	g_s	Leaf stomatal conductance to water vapor.	-	mol m^{-2} s^{-1}
	g_{tot}	Total leaf conductance to water vapor.	-	mol m^{-2} s^{-1}
	g_R	Leaf conductance to radiative heat transfer.	-	mol m^{-2} s^{-1}
	A	Leaf gross photosynthesis.	-	µmol CO_2 m^{-2} s^{-1}`
Canopy properties	ϵ_{sky}	Sky emissivity.	-	-
	LW_{top}	Top-of-canopy downwelling longwave radiation.	-	W m^{-2}
	SW_{top}	Top-of-canopy downwelling shortwave radiation.	-	W m^{-2}
	f	Proportion of diffuse shortwave radiation at the top of the canopy.	-	-
	f_{ET}	Ratio of actual evapotranspiration to potential evapotranspiration.	-	-
	GPP	Canopy gross primary production.	-	µmol CO_2 m^{-2} s^{-1}
	G_c	Canopy conductance to water vapor.	-	mol m^{-2} s^{-1}

832

Table S2: Model goodness-of-fit statistics for mixed effects modeling. Models were derived from midday averages as in Figure S9. AIC: Akaike information criterion.

Formula	N parameters	AIC	Log-likelihood
$T_L \sim (T_A - 1 \mid \text{site})$	3	2,750.9	-1,372.4
$T_L \sim (T_A + T_A : f_{ET} - 1 \mid \text{site})$	5	2,464.3	-1,227.2

836 Table S3: Random effects by site for the linear mixed effects model fit with an interaction term.

Site	Leaf-air temperature slope, $f_{ET} = 0$	Water availability interaction term	Leaf-air temperature slope, $f_{ET} = 1$
TALL	0.975	0.003	0.978
JERC	1.020	-0.037	0.982
WREF	1.038	-0.192	0.847
OSBS	1.043	-0.085	0.957
DEJU	1.120	-0.243	0.877
ABBY	1.151	-0.224	0.928
RMNP	1.234	-0.291	0.942

837

838 Table S4: NEON data product metadata.

Data Product ID	Data Product Name	DOI	Site IDs	Date Range
DP1.10017.001	Digital hemispheric photos of plot vegetation	https://doi.org/10.48443/jbb9-2t38	ABBY, DEJU, JERC, OSBS, RMNP, TALL, WREF	2019-04-23 – 2019-07-02
DP1.30003.001	Discrete return lidar point cloud	https://doi.org/10.48443/xxby-5a18	ABBY, DEJU, JERC, OSBS, RMNP, TALL, WREF	2021-05-01 – 2021-09-01
DP4.00200.001	Bundled data products – eddy covariance	https://doi.org/10.48443/2ms3-a333	ABBY, DEJU, JERC, OSBS, RMNP, TALL, WREF	2018-05-03 – 2021-09-30

839

840

841 Table S5: Ameriflux BASE data product metadata.

Ameriflux Site ID	Site Name	DOI
US-xAB	NEON Abby Road (ABBY)	https://doi.org/10.17190/AMF/1617726
US-xDJ	NEON Delta Junction (DEJU)	https://doi.org/10.17190/AMF/1634884
US-xJE	NEON Jones Ecological Research Center (JERC)	https://doi.org/10.17190/AMF/1617730
US-xRM	NEON Rocky Mountain National Park, CASTNET (RMNP)	https://doi.org/10.17190/AMF/1579723
US-xSB	NEON Ordway-Swisher Biological Station (OSBS)	https://doi.org/10.17190/AMF/1671899
US-xTA	NEON Talladega National Forest (TALL)	https://doi.org/10.17190/AMF/1671902
US-xWR	NEON Wind River Experimental Forest (WREF)	https://doi.org/10.17190/AMF/1617742

842

843

References

Anderegg, W.R.L., Kane, J.M., Anderegg, L.D.L., 2013. Consequences of widespread tree mortality triggered by drought and temperature stress. Nature Clim Change 3, 30–36. https://doi.org/10.1038/nclimate1635

Aubrecht, D.M., Helliker, B.R., Goulden, M.L., Roberts, D.A., Still, C.J., Richardson, A.D., 2016. Continuous, long-term, high-frequency thermal imaging of vegetation: Uncertainties and recommended best practices. Agricultural and Forest Meteorology 228–229, 315–326. https://doi.org/10.1016/j.agrformet.2016.07.017

Bates, D., Mächler, M., Bolker, B., Walker, S., 2015. Fitting Linear Mixed-Effects Models Using lme4. Journal of Statistical Software 67, 1–48. https://doi.org/10.18637/jss.v067.i01

Blonder, B., Michaletz, S.T., 2018. A model for leaf temperature decoupling from air temperature. Agricultural and Forest Meteorology 262, 354–360. https://doi.org/10.1016/j.agrformet.2018.07.012

Cavaleri, M.A., 2020. Cold-blooded forests in a warming world. New Phytologist 228, 1455–1457. https://doi.org/10.1111/nph.16916

Cawse-Nicholson, K., Townsend, P.A., Schimel, D., Assiri, A.M., Blake, P.L., Buongiorno, M.F., Campbell, P., Carmon, N., Casey, K.A., Correa-Pabón, R.E., Dahlin, K.M., Dashti, H., Dennison, P.E., Dierssen, H., Erickson, A., Fisher, J.B., Frouin, R., Gatebe, C.K., Gholizadeh, H., Gierach, M., Glenn, N.F., Goodman, J.A., Griffith, D.M., Guild, L., Hakkenberg, C.R., Hochberg, E.J., Holmes, T.R.H., Hu, C., Hulley, G., Huemmrich, K.F., Kudela, R.M., Kokaly, R.F., Lee, C.M., Martin, R., Miller, C.E., Moses, W.J., Muller-Karger, F.E., Ortiz, J.D., Otis, D.B., Pahlevan, N., Painter, T.H., Pavlick, R., Poulter, B., Qi, Y., Realmuto, V.J., Roberts, D., Schaepman, M.E., Schneider, F.D., Schwandner, F.M., Serbin, S.P., Shiklomanov, A.N., Stavros, E.N., Thompson, D.R., Torres-Perez, J.L., Turpie, K.R., Tzortziou, M., Ustin, S., Yu, Q., Yusup, Y., Zhang, Q., 2021. NASA's surface biology and geology designated observable: A perspective on surface imaging algorithms. Remote Sensing of Environment 257, 112349. https://doi.org/10.1016/j.rse.2021.112349

Chen, Y.-Y., Wang, S.-Y.S., Yu, H., Liu, W.-Y., 2024. When forests hold their breath: will increasing drought further disrupt carbon sequestration? Environ. Res. Lett. https://doi.org/10.1088/1748-9326/ad27ba

Choat, B., Brodribb, T.J., Brodersen, C.R., Duursma, R.A., López, R., Medlyn, B.E., 2018. Triggers of tree mortality under drought. Nature 558, 531–539. https://doi.org/10.1038/s41586-018-0240-x

Cook, A.M., Berry, N., Milner, K.V., Leigh, A., 2021. Water availability influences thermal safety margins for leaves. Functional Ecology 35, 2179–2189. https://doi.org/10.1111/1365-2435.13868

Coop, J.D., Parks, S.A., Stevens-Rumann, C.S., Crausbay, S.D., Higuera, P.E., Hurteau, M.D., Tepley, A., Whitman, E., Assal, T., Collins, B.M., Davis, K.T., Dobrowski, S., Falk, D.A., Fornwalt, P.J., Fulé, P.Z., Harvey, B.J., Kane, V.R., Littlefield, C.E., Margolis, E.Q., North, M., Parisien, M.-A., Prichard, S., Rodman, K.C., 2020. Wildfire-Driven Forest Conversion in Western North American Landscapes. BioScience 70, 659–673. https://doi.org/10.1093/biosci/biaa061

Doughty, C.E., Keany, J.M., Wiebe, B.C., Rey-Sanchez, C., Carter, K.R., Middleby, K.B., Cheesman, A.W., Goulden, M.L., da Rocha, H.R., Miller, S.D., Malhi, Y., Fauset, S.,

Gloor, E., Slot, M., Oliveras Menor, I., Crous, K.Y., Goldsmith, G.R., Fisher, J.B., 2023. Tropical forests are approaching critical temperature thresholds. Nature 1–7. https://doi.org/10.1038/s41586-023-06391-z

Drake, J.E., Harwood, R., Vårhammar, A., Barbour, M.M., Reich, P.B., Barton, C.V.M., Tjoelker, M.G., 2020. No evidence of homeostatic regulation of leaf temperature in Eucalyptus parramattensis trees: integration of CO2 flux and oxygen isotope methodologies. New Phytologist 228, 1511–1523. https://doi.org/10.1111/nph.16733

Fisher, J.B., Lee, B., Purdy, A.J., Halverson, G.H., Dohlen, M.B., Cawse-Nicholson, K., Wang, A., Anderson, R.G., Aragon, B., Arain, M.A., Baldocchi, D.D., Baker, J.M., Barral, H., Bernacchi, C.J., Bernhofer, C., Biraud, S.C., Bohrer, G., Brunsell, N., Cappelaere, B., Castro-Contreras, S., Chun, J., Conrad, B.J., Cremonese, E., Demarty, J., Desai, A.R., De Ligne, A., Foltýnová, L., Goulden, M.L., Griffis, T.J., Grünwald, T., Johnson, M.S., Kang, M., Kelbe, D., Kowalska, N., Lim, J.-H., Maïnassara, I., McCabe, M.F., Missik, J.E.C., Mohanty, B.P., Moore, C.E., Morillas, L., Morrison, R., Munger, J.W., Posse, G., Richardson, A.D., Russell, E.S., Ryu, Y., Sanchez-Azofeifa, A., Schmidt, M., Schwartz, E., Sharp, I., Šigut, L., Tang, Y., Hulley, G., Anderson, M., Hain, C., French, A., Wood, E., Hook, S., 2020. ECOSTRESS: NASA's Next Generation Mission to Measure Evapotranspiration From the International Space Station. Water Resources Research 56, e2019WR026058. https://doi.org/10.1029/2019WR026058

Gardner, B.R., Blad, B.L., Watts, D.G., 1981. Plant and air temperatures in differentially-irrigated corn. Agricultural Meteorology 25, 207–217. https://doi.org/10.1016/0002-1571(81)90073-X

Garen, J.C., Aparecido, L.M.T., Blonder, B.W., Cavaleri, M.A., Slot, M., Michaletz, S.T., 2023. Canopy-top measurements do not accurately quantify canopy-scale leaf thermoregulation. Proceedings of the National Academy of Sciences 120, e2301914120. https://doi.org/10.1073/pnas.2301914120

Garen, J.C., Branch, H.A., Borrego, I., Blonder, B., Stinziano, J.R., Michaletz, S.T., 2022. Gas exchange analysers exhibit large measurement error driven by internal thermal gradients. New Phytologist 236, 369–384. https://doi.org/10.1111/nph.18347

Gauthey, A., Bachofen, C., Deluigi, J., Didion-Gency, M., D'Odorico, P., Gisler, J., Mas, E., Schaub, M., Schuler, P., Still, C.J., Tunas, A., Grossiord, C., 2023. Absence of canopy temperature variation despite stomatal adjustment in *Pinus sylvestris* under multidecadal soil moisture manipulation. New Phytologist nph.19136. https://doi.org/10.1111/nph.19136

Gough, C.M., Atkins, J.W., Fahey, R.T., Hardiman, B.S., 2019. High rates of primary production in structurally complex forests. Ecology 100, e02864. https://doi.org/10.1002/ecy.2864

Griffani, D.S., Rognon, P., Farquhar, G.D., 2024. The role of thermodiffusion in transpiration. New Phytologist nph.19642. https://doi.org/10.1111/nph.19642

Guo, Z., Still, C.J., Lee, C.K.F., Ryu, Y., Blonder, B., Wang, J., Bonebrake, T.C., Hughes, A., Li, Y., Yeung, H.C.H., Zhang, K., Law, Y.K., Lin, Z., Wu, J., 2023a. Does plant ecosystem thermoregulation occur? An extratropical assessment at different spatial and temporal scales. New Phytologist 238, 1004–1018. https://doi.org/10.1111/nph.18632

Guo, Z., Zhang, K., Lin, H., Majcher, B.M., Lee, C.K.F., Still, C.J., Wu, J., 2023b. Plant canopies exhibit stronger thermoregulation capability at the seasonal than diurnal timescales. Agricultural and Forest Meteorology 339, 109582. https://doi.org/10.1016/j.agrformet.2023.109582

Idso, S.B., Jackson, R.D., Pinter, P.J., Reginato, R.J., Hatfield, J.L., 1981. Normalizing the stress-degree-day parameter for environmental variability. Agricultural Meteorology 24, 45–55. https://doi.org/10.1016/0002-1571(81)90032-7

Jarvis, P.G., McNaughton, K.G., 1986. Stomatal Control of Transpiration: Scaling Up from Leaf to Region, in: Advances in Ecological Research. Elsevier, pp. 1–49. https://doi.org/10.1016/S0065-2504(08)60119-1

Javadian, M., Smith, W.K., Lee, K., Knowles, J.F., Scott, R.L., Fisher, J.B., Moore, D.J.P., van Leeuwen, W.J.D., Barron-Gafford, G., Behrangi, A., 2022. Canopy Temperature Is Regulated by Ecosystem Structural Traits and Captures the Ecohydrologic Dynamics of a Semiarid Mixed Conifer Forest Site. Journal of Geophysical Research: Biogeosciences 127, e2021JG006617. https://doi.org/10.1029/2021JG006617

Jiang, Y., Kim, J.B., Trugman, A.T., Kim, Y., Still, C.J., 2019. Linking tree physiological constraints with predictions of carbon and water fluxes at an old-growth coniferous forest. Ecosphere 10, e02692. https://doi.org/10.1002/ecs2.2692

Jones, H.G., 2013. Plants and Microclimate: A Quantitative Approach to Environmental Plant Physiology, 3rd ed. Cambridge University Press. https://doi.org/10.1017/CBO9780511845727

Kerhoulas, L.P., Weisgrau, A.S., Hoeft, E.C., Kerhoulas, N.J., 2020. Vertical gradients in foliar physiology of tall Picea sitchensis trees. Tree Physiol 40, 321–332. https://doi.org/10.1093/treephys/tpz137

Kibler, C.L., Trugman, A.T., Roberts, D.A., Still, C.J., Scott, R.L., Caylor, K.K., Stella, J.C., Singer, M.B., 2023. Evapotranspiration regulates leaf temperature and respiration in dryland vegetation. Agricultural and Forest Meteorology 339, 109560. https://doi.org/10.1016/j.agrformet.2023.109560

Kim, Y., Still, C.J., Roberts, D.A., Goulden, M.L., 2018. Thermal infrared imaging of conifer leaf temperatures: Comparison to thermocouple measurements and assessment of environmental influences. Agricultural and Forest Meteorology 248, 361–371. https://doi.org/10.1016/j.agrformet.2017.10.010

Knauer, J., Zaehle, S., Medlyn, B.E., Reichstein, M., Williams, C.A., Migliavacca, M., De Kauwe, M.G., Werner, C., Keitel, C., Kolari, P., Limousin, J.-M., Linderson, M.-L., 2018. Towards physiologically meaningful water-use efficiency estimates from eddy covariance data. Global Change Biology 24, 694–710. https://doi.org/10.1111/gcb.13893

Körner, C., Hiltbrunner, E., 2018. The 90 ways to describe plant temperature. Perspectives in Plant Ecology, Evolution and Systematics, Special issue on Alpine and arctic plant communities : a worldwide perspective 30, 16–21. https://doi.org/10.1016/j.ppees.2017.04.004

Leuzinger, S., Körner, C., 2007. Tree species diversity affects canopy leaf temperatures in a mature temperate forest. Agricultural and Forest Meteorology 146, 29–37. https://doi.org/10.1016/j.agrformet.2007.05.007

Li, X., Gentine, P., Lin, C., Zhou, S., Sun, Z., Zheng, Y., Liu, J., Zheng, C., 2019. A simple and objective method to partition evapotranspiration into transpiration and evaporation at eddy-covariance sites. Agricultural and Forest Meteorology 265, 171–182. https://doi.org/10.1016/j.agrformet.2018.11.017

Lin, H., Chen, Y., Zhang, H., Fu, P., Fan, Z., 2017. Stronger cooling effects of transpiration and leaf physical traits of plants from a hot dry habitat than from a hot wet habitat. Functional Ecology 31, 2202–2211. https://doi.org/10.1111/1365-2435.12923

Linacre, E.T., 1964. A note on a feature of leaf and air temperatures. Agricultural Meteorology 1, 66–72. https://doi.org/10.1016/0002-1571(64)90009-3
Liu, M., Trugman, A.T., Peñuelas, J., Anderegg, W.R.L., 2024. Climate-driven disturbances amplify forest drought sensitivity. Nat. Clim. Chang. 1–7. https://doi.org/10.1038/s41558-024-02022-1
Maechler, M., Rousseeuw, P., Croux, C., Todorov, V., Ruckstuhl, A., Salibian-Barrera, M., Verbeke, T., Koller, M., Conceicao, E.L.T., Anna di Palma, M., 2024. robustbase: Basic robust statistics (manual).
Mahan, J.R., Upchurch, D.R., 1988. Maintenance of constant leaf temperature by plants—I. Hypothesis-limited homeothermy. Environmental and Experimental Botany 28, 351–357. https://doi.org/10.1016/0098-8472(88)90059-7
Marchin, R.M., Backes, D., Ossola, A., Leishman, M.R., Tjoelker, M.G., Ellsworth, D.S., 2022. Extreme heat increases stomatal conductance and drought-induced mortality risk in vulnerable plant species. Global Change Biology 28, 1133–1146. https://doi.org/10.1111/gcb.15976
Marchin, R.M., Medlyn, B.E., Tjoelker, M.G., Ellsworth, D.S., 2023. Decoupling between stomatal conductance and photosynthesis occurs under extreme heat in broadleaf tree species regardless of water access. Global Change Biology 29, 6319–6335. https://doi.org/10.1111/gcb.16929
Marshall, B., Biscoe, P.V., 1980. A Model for C3 Leaves Describing the Dependence of Net Photosynthesis on Irradiance. Journal of Experimental Botany 31, 29–39. https://doi.org/10.1093/jxb/31.1.29
Medlyn, B.E., De Kauwe, M.G., Lin, Y., Knauer, J., Duursma, R.A., Williams, C.A., Arneth, A., Clement, R., Isaac, P., Limousin, J., Linderson, M., Meir, P., Martin-StPaul, N., Wingate, L., 2017. How do leaf and ecosystem measures of water-use efficiency compare? New Phytologist 216, 758–770. https://doi.org/10.1111/nph.14626
Medlyn, B.E., Duursma, R.A., Eamus, D., Ellsworth, D.S., Prentice, I.C., Barton, C.V.M., Crous, K.Y., De Angelis, P., Freeman, M., Wingate, L., 2011. Reconciling the optimal and empirical approaches to modelling stomatal conductance. Global Change Biology 17, 2134–2144. https://doi.org/10.1111/j.1365-2486.2010.02375.x
Michaletz, S.T., Weiser, M.D., McDowell, N.G., Zhou, J., Kaspari, M., Helliker, B.R., Enquist, B.J., 2016. The energetic and carbon economic origins of leaf thermoregulation. Nature Plants 2, 1–9. https://doi.org/10.1038/nplants.2016.129
Miller, B.D., Carter, K.R., Reed, S.C., Wood, T.E., Cavaleri, M.A., 2021. Only sun-lit leaves of the uppermost canopy exceed both air temperature and photosynthetic thermal optima in a wet tropical forest. Agricultural and Forest Meteorology 301–302, 108347. https://doi.org/10.1016/j.agrformet.2021.108347
Monteith, J.L., Unsworth, M.H., 2013. Principles of environmental physics: plants, animals, and the atmosphere, 4th ed. ed. Elsevier/Academic Press, Amsterdam ; Boston.
Muller, J.D., Rotenberg, E., Tatarinov, F., Oz, I., Yakir, D., 2021. Evidence for efficient nonevaporative leaf-to-air heat dissipation in a pine forest under drought conditions. New Phytologist 232, 2254–2266. https://doi.org/10.1111/nph.17742
Okajima, Y., Taneda, H., Noguchi, K., Terashima, I., 2012. Optimum leaf size predicted by a novel leaf energy balance model incorporating dependencies of photosynthesis on light and temperature. Ecol Res 27, 333–346. https://doi.org/10.1007/s11284-011-0905-5

Pau, S., Detto, M., Kim, Y., Still, C.J., 2018. Tropical forest temperature thresholds for gross primary productivity. Ecosphere 9, e02311. https://doi.org/10.1002/ecs2.2311
Posch, B.C., Bush, S.E., Koepke, D.F., Schuessler, A., Anderegg, L.L.D., Aparecido, L.M.T., Blonder, B.W., Guo, J.S., Kerr, K.L., Moran, M.E., Cooper, H.F., Doughty, C.E., Gehring, C.A., Whitham, T.G., Allan, G.J., Hultine, K.R., 2024. Intensive leaf cooling promotes tree survival during a record heatwave. Proceedings of the National Academy of Sciences 121, e2408583121. https://doi.org/10.1073/pnas.2408583121
Rastogi, B., Schmidt, A., Berkelhammer, M., Noone, D., Meinzer, F.C., Kim, J., Still, C.J., 2022. Enhanced Photosynthesis and Transpiration in an Old Growth Forest Due To Wildfire Smoke. Geophysical Research Letters 49, e2022GL097959. https://doi.org/10.1029/2022GL097959
Ruelland, E., Zachowski, A., 2010. How plants sense temperature. Environmental and Experimental Botany 69, 225–232. https://doi.org/10.1016/j.envexpbot.2010.05.011
Smigaj, M., Gaulton, R., Suarez, J.C., Barr, S.L., 2017. Use of Miniature Thermal Cameras for Detection of Physiological Stress in Conifers. Remote Sensing 9, 957. https://doi.org/10.3390/rs9090957
Sprintsin, M., Chen, J.M., Czurylowicz, P., 2011. Combining land surface temperature and shortwave infrared reflectance for early detection of mountain pine beetle infestations in western Canada. JARS 5, 053566. https://doi.org/10.1117/1.3662866
Stark, S.C., Leitold, V., Wu, J.L., Hunter, M.O., de Castilho, C.V., Costa, F.R.C., McMahon, S.M., Parker, G.G., Shimabukuro, M.T., Lefsky, M.A., Keller, M., Alves, L.F., Schietti, J., Shimabukuro, Y.E., Brandão, D.O., Woodcock, T.K., Higuchi, N., de Camargo, P.B., de Oliveira, R.C., Saleska, S.R., 2012. Amazon forest carbon dynamics predicted by profiles of canopy leaf area and light environment. Ecology Letters 15, 1406–1414. https://doi.org/10.1111/j.1461-0248.2012.01864.x
Still, C.J., Page, G., Rastogi, B., Griffith, D.M., Aubrecht, D.M., Kim, Y., Burns, S.P., Hanson, C.V., Kwon, H., Hawkins, L., Meinzer, F.C., Sevanto, S., Roberts, D., Goulden, M., Pau, S., Detto, M., Helliker, B., Richardson, A.D., 2022. No evidence of canopy-scale leaf thermoregulation to cool leaves below air temperature across a range of forest ecosystems. Proc. Natl. Acad. Sci. U.S.A. 119, e2205682119. https://doi.org/10.1073/pnas.2205682119
Still, C.J., Page, G.F.M., Rastogi, B., Griffith, D.M., Aubrecht, D.M., Kim, Y., Burns, S.P., Hanson, C.V., Kwon, H., Hawkins, L., Meinzer, F.C., Sevanto, S., Roberts, D.A., Goulden, M., Pau, S., Detto, M., Helliker, B.R., Richardson, A.D., 2023a. Reply to Garen et al.: Within-canopy temperature data also do not support limited homeothermy. Proceedings of the National Academy of Sciences 120, e2302515120. https://doi.org/10.1073/pnas.2302515120
Still, C.J., Powell, R., Aubrecht, D., Kim, Y., Helliker, B., Roberts, D., Richardson, A.D., Goulden, M., 2019a. Thermal imaging in plant and ecosystem ecology: applications and challenges. Ecosphere 10, e02768. https://doi.org/10.1002/ecs2.2768
Still, C.J., Sibley, A., DePinte, D., Busby, P.E., Harrington, C.A., Schulze, M., Shaw, D.R., Woodruff, D., Rupp, D.E., Daly, C., Hammond, W.M., Page, G.F.M., 2023b. Causes of widespread foliar damage from the June 2021 Pacific Northwest Heat Dome: more heat than drought. Tree Physiology 43, 203–209. https://doi.org/10.1093/treephys/tpac143
Still, C.J., Sibley, A., Page, G., Meinzer, F.C., Sevanto, S., 2019b. When a cuvette is not a canopy: A caution about measuring leaf temperature during gas exchange measurements.

Agricultural and Forest Meteorology 279, 107737. https://doi.org/10.1016/j.agrformet.2019.107737
Stinziano, J.R., Roback, C., Sargent, D., Murphy, B.K., Hudson, P.J., Muir, C.D., 2021. Principles of resilient coding for plant ecophysiologists. AoB Plants 13, plab059. https://doi.org/10.1093/aobpla/plab059
Upchurch, D.R., Mahan, J.R., 1988. Maintenance of constant leaf temperature by plants—II. Experimental observations in cotton. Environmental and Experimental Botany 28, 359–366. https://doi.org/10.1016/0098-8472(88)90060-3
Vinod, N., Slot, M., McGregor, I.R., Ordway, E.M., Smith, M.N., Taylor, T.C., Sack, L., Buckley, T.N., Anderson-Teixeira, K.J., 2023. Thermal sensitivity across forest vertical profiles: patterns, mechanisms, and ecological implications. New Phytologist 237, 22–47. https://doi.org/10.1111/nph.18539
Wang, Y.-P., Leuning, R., 1998. A two-leaf model for canopy conductance, photosynthesis and partitioning of available energy I:: Model description and comparison with a multi-layered model. Agricultural and Forest Meteorology 91, 89–111. https://doi.org/10.1016/S0168-1923(98)00061-6
Williams, A.P., Abatzoglou, J.T., Gershunov, A., Guzman-Morales, J., Bishop, D.A., Balch, J.K., Lettenmaier, D.P., 2019. Observed Impacts of Anthropogenic Climate Change on Wildfire in California. Earth's Future 7, 892–910. https://doi.org/10.1029/2019EF001210
Williams, C.A., Gu, H., MacLean, R., Masek, J.G., Collatz, G.J., 2016. Disturbance and the carbon balance of US forests: A quantitative review of impacts from harvests, fires, insects, and droughts. Global and Planetary Change 143, 66–80. https://doi.org/10.1016/j.gloplacha.2016.06.002
Winner, W.E., Thomas, S.C., Berry, J.A., Bond, B.J., Cooper, C.E., Hinckley, T.M., Ehleringer, J.R., Fessenden, J.E., Lamb, B., McCarthy, S., McDowell, N.G., Phillips, N., Williams, M., 2004. Canopy Carbon Gain and Water Use: Analysis of Old-growth Conifers in the Pacific Northwest. Ecosystems 7, 482–497. https://doi.org/10.1007/s10021-004-0139-2
Wutzler, T., Lucas-Moffat, A., Migliavacca, M., Knauer, J., Sickel, K., Šigut, L., Menzer, O., Reichstein, M., 2018. Basic and extensible post-processing of eddy covariance flux data with REddyProc. Biogeosciences 15, 5015–5030. https://doi.org/10.5194/bg-15-5015-2018
Zakrzewska, A., Kopeć, D., 2022. Remote sensing of bark beetle damage in Norway spruce individual tree canopies using thermal infrared and airborne laser scanning data fusion. Forest Ecosystems 100068. https://doi.org/10.1016/j.fecs.2022.100068
Zhou, Y., Kitudom, N., Fauset, S., Slot, M., Fan, Z., Wang, J., Liu, W., Lin, H., 2023. Leaf thermal regulation strategies of canopy species across four vegetation types along a temperature and precipitation gradient. Agricultural and Forest Meteorology 343, 109766. https://doi.org/10.1016/j.agrformet.2023.109766